이 학 석 사 학 위 논 문

Carbon Dioxide Capture By Using Pore-Modified Porous Organic Polymers

동공을 변형시킨 다공성 유기 고분자를 이용한 이산화탄소 포집 연구

2014년 2월

서울대학교 대학원

화학부 무기화학 전공

성 시 영

Carbon Dioxide Capture By Using Pore-Modified Porous Organic Polymers

By

Siyoung Sung

Supervisor: Prof. Myunghyun Paik Suh

A Thesis for the M.S. Degree

in Inorganic Chemistry

Department of Chemistry

Graduate School

Seoul National University

Feburary, 2014

이 학 석 사 학 위 논 문

Carbon Dioxide Capture By Using Pore-Modified Porous Organic Polymers

동공을 변형시킨 다공성 유기 고분자를 이용한 이산화탄소 포집 연구

지도교수 백 명 현

이 논문을 이학석사학위논문으로 제출함

2013년 12월

서울대학교 대학원

화학부 무기화학 전공

성 시 영

성시영의 석사학위 논문을 인준함

2014년 2월

위 원 장 _____ (인)

부 위 원 장 _____ (인)

위 원 _____ (인)

Abstract

Carbon Dioxide Capture By Using Pore-Modified Porous Organic Polymers

In order to mitigate the recent environmental crises such as global warming, climate change, and ocean acidification, the development of an efficient carbon dioxide (CO_2) capture technology from flue gas is very important.[1-4] Industrial flue gas is mainly composed of N_2 (75%), CO_2 (15%), and other gases including water vapor with a temperature between 313 to 333 K.[1] Therefore, it is important to develop a material with a high adsorption selectivity for CO_2 over N_2 at a low CO_2 partial pressure, outstanding water stability, as well as a high CO_2 uptake capacity at elevated temperatures.[1] Porous Organic Polymers (POPs) have gained significant attention as a class of promising CO_2 capture material due to their superior physical properties such as high surface areas, extremely low density, and excellent thermal, chemical and water stability.[5-9] In particular, the low density of porous organic polymers achieved by covalent bonds of only light elements such as C, N and H results in a high CO_2 uptake per g unit mass of adsorbent.[8,9] In addition, the polymers display superior stability against water,[10] which is crucial for a post combustion CO_2 capture material. Therefore, porous organic materials have the potential to be the optimal class of CO_2 capture materials provided that their selectivity for CO_2 over N_2 are also high. In this study, PAF-5, a porous organic polymerl having both low density and excellent water stability, was impregnated with branched polyethylenimine (PEI, M_W = *ca.* 800) to increase the CO_2 uptake capacity and adsorption selectivity for CO_2 over N_2. PAF-5 with a 2D layered hexagonal structure constructed from only phenyl rings displays a

high surface area (BET: 1503 m^2 g^{-1}) as well as a large pore width (1.66 nm) and pore volume (1.35 cc g^{-1}).[11] We expected that numerous amine functional groups of PEI dispersed in the large 1D channels of PAF-5 might act as strong CO_2 interaction sites. In particular, PEI(40 wt%)⊂PAF-5 adsorbed 10.0 wt% of CO_2 under a stream of 15% (v/v) CO_2 in N_2 at 313 K within 20 minutes. The adsorbent was completely regenerated within 20 minutes at 343 K under a N_2 flow. Even after 10 cycles of adsorption and desorption, PEI(40 wt%)⊂PAF-5 did not show any decrease in the CO_2 uptake capacity or decomposition of the adsorbent. In addition, after exposure to water vapor for 7 days at 313 K, the material still adsorbed almost the same amount of CO_2 under the aforementioned conditions, which also proves its superior stability against water.

Keywords: porous organic polymer • polyethylenimine • •carbon dioxide capture • gas cycling experiment • isosteric heat of adsorption

Table of contents

I. Introduction

In 2007, the Intergovernmental Panel on Climate Change (IPCC) reported that global warming was increasing at an accelerating rate due to the escalating level of atmospheric carbon dioxide. The rapid acceleration of worldwide industrialization over last century resulted in dramatic increase in the level of the earth's atmospheric carbon dioxide (CO_2), one of the primary greenhouse gases responsible for recent global warming phenomenon. According to Monthly Mean Concentrations at the Mauna Loa Observatory, The concentration of atmospheric CO_2 has increased from about 316 ppm in 1958 to about 396 ppm in 2012.[12] The anthropogenic emission of CO_2 is mainly caused by the combustion of carbon-based fossil fuels such as coal, oil, and natural gas and expected to be escalated considering current industries' significant dependence on fossil fuels as their major energy sources. To make matters worse, the climate change caused by increase in CO_2 concentration is expected to be predominantly irreversible for 1,000 years after emissions stop.[13] Becoming aware of the seriousness of anthropogenic CO_2 discharge, interconnected international communities have been putting an effort to reduce the atmospheric concentration of CO_2. For instance, The Kyoto Protocol was adopted by the UN in 1997. Under the Protocol, 37 countries committed themselves to reducing the emission of four different greenhouse gases (GHG), including CO_2. For the further action, the U.S. Department of Energy (DOE) initiated The Carbon Sequestration Program setting the following major goals:[14] 1) Develop technologies that can separate, capture, transport, and store CO_2 using either direct or indirect systems that result in a less than 10 percent increase in the cost of energy at pre-combustion power plants by 2015. 2) Develop technologies that will support industries' ability to predict CO_2 storage

capacity in geologic formations to within ±30 by 2015.

In the long term perspective, it is indispensable to replace fossil fuels with cleaner and sustainable energy sources such as hydrogen and solar energy to mitigate atmospheric CO_2 concentration. However, current technologies utilizing these alternative energy sources are still in their infancy and require intensive optimization to completely substitute fossil fuels. In addition, it takes at least several decades by putting a great economic cost to ultimately transform the existing coal-fired power plants into the power plants utilizing alternative energy sources. Therefore, development of the technologies for cost-efficient Carbon Capture and Sequestration (CCS) becomes very important. CCS mainly consists of three processes. Typical coal-fired power plants emit flue gas containing ~78% N_2 from the atmosphere, ~15% CO_2 in the hydrocarbon, and 7% water.[15] For the first process of CCS, CO_2 gas should be selectively captured from the flue gas. The separated CO_2 gas is then compressed into the concentrated CO_2 stream and transported via pipelines to suitable sequestration sites. Finally, the transported CO_2 stream is injected into a geologic formation permanently. Although transportation and sequestration of CO_2 are already well established processes in CCS, developing technologies to selectively capture CO_2 from flue gas is in a nascent stage. Moreover, it is CO_2 capture step that consumes the most energy resulting in the highest cost in CCS process.[16] Hence, establishing highly efficient CO_2 capture technologies is essential for commercialization of CCS.

I. 1. Three different strategies of CO_2 capture from power plants.

For the effective capture of CO_2 from coal-fired power plants, there exist three distinctive fundamental approaches including pre-combustion capture, post-combustion capture and oxy-fuel combustion. These three different strategies of CO_2 capture are illustrated in Figure 1.[17]

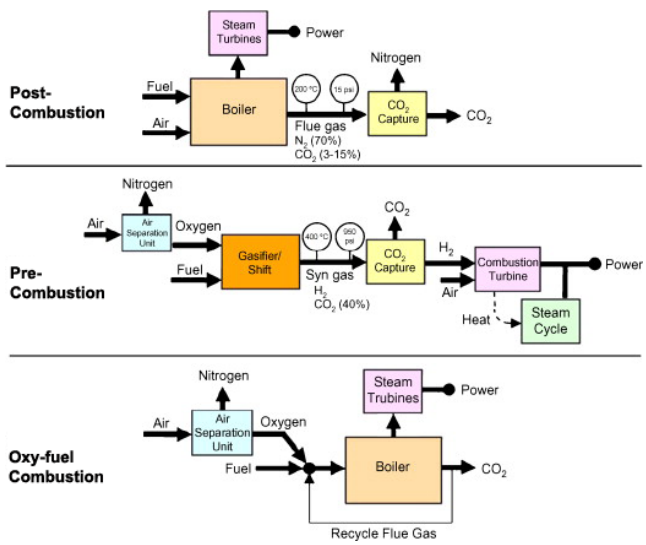

Figure.1 A schematic illustration of three distinctive CO_2 capture methods.

Pre-combustion capture of CO_2 has arrested recent attention as a cost-effective means of CO_2 capture.[18] In pre-combustion, CO_2 is separated from a mixture gas of mainly CO_2 and H_2 prior to the combustion of fossil fuels. For the pre-combustion capture of CO_2, two essential technologies, which include integrated gasification combine cycle (IGCC) and shift conversion are required.[17] With IGCC technology, coal is first gasified with oxygen (partial oxidation) producing synthesis gas, a gas mixture composed of primarily CO and H_2. The resultant synthesis gas is

then sent to a shift converter so that CO can go through the water gas shift reaction in which CO is reacted with water resulting in CO_2 and H_2. The resulting mixture gas is called from which CO_2 is separated. After separation of CO_2 from the shifted synthesis gas, pure hydrogen and carbon dioxide streams are made and the former is subject to combustion for power generation and the latter to permanent storage. Since shifted synthesis gas has high pressure as well as high CO_2 partial pressure, CO_2 can be readily separated from the mixture gas. Another advantage that pre-combustion CO_2 capture holds is reduction in cost required for the compression of separated CO_2 due to the high pressure of shifted synthesis gas.[17]

Post-combustion capture of CO_2 is the most dominantly applied CO_2 capture strategy for coal-fired power plants since the facilities of post-combustion capture can be retrofitted to the existing power plants with greater ease. In post-combustion CO_2 capture, contrary to the pre-combustion CO_2 capture, CO_2 is removed from the flue gas produced by the combustion of fossil fuels in air. The resulting flue gas has a total pressure of approximately 1 atm and is mainly composed of N_2 and CO_2. The partial pressure of N_2 is *ca.* 0.75 atm and that of CO_2 is *ca.* 0.15 atm. Since the primary constituents of the flue gas from power plants are N_2 and CO_2, high selectivity for CO_2 over N_2 at ambient temperature and atmospheric pressure is required to be a successful solid adsorbent to capture CO_2 in post-combustion capture. One of the advantages that post-combustion capture of CO_2 has is its great applicability to the majority of existing coal-fired power plants. Post-combustion capture of CO_2 with aqueous alkanolamine solutions is being extensively exploited recently. However, one major drawback of this CO_2 capture approach, which is derived from low CO_2 partial pressure in flue gas is that significantly higher performance or circulation volume of

capture materials is required for high capture level.[17]

Oxy-fuel combustion employs a new combustion environment to mitigate CO_2 emission from fossil-fuel power stations. Power plants with oxy-fuel combustion installation ignite pulverized coal (PC) with nearly pure oxygen (purity greater than 95%) so that the resulting flue gas is mainly comprised of CO_2 and water vapor. Water vapor in flue gas can be condensed and easily separated from CO_2 and the flue gas is ready for sequestration without stripping CO_2 from the flue gas. In oxy-fuel combustion, providing highly pure O_2 for combustion of fossil fuels is a mightily important process conducted by a cryogenic air separation unit. The high purity oxygen separated from dry air in a cryogenic air separation unit is mixed with recycled flue gas prior to combustion to control high flame temperature and provide enough gas to carry the heat through a boiler.[19] One significant advantage that oxy-fuel combustion provides is high CO_2 concentration in flue gas. By utilizing oxy-fuel combustion, the CO_2 concentration can be increased from approximately 17 to 70 % by mass.[20] In spite of the great benefit, a major problem of oxy-fuel combustion is that this combustion method requires cost-prohibitive large cryogenic O_2 production.[17] Under the circumstances, developing materials that selectively adsorb O_2 over N_2 is necessary for commercialization of oxy-fuel combustion. Metal organic frameworks with high O_2 selectivity are suggested to be a promising class of materials for selective O_2 capture.

I. 2. Current CO_2 capture technology

Amine scrubbing is the most commercially mature CO_2 capture technology at large-scale point sources. It is also expected to be the dominant technology forpost-combustion capture of CO_2 from flue gas emitted by coal-fired power plants even in 2030 unless more cost-effective technology is developed.[16] Amine-based CCS system is comprised of two primary elements. One of the two coreparts is an absorber where aqueous alkanolamine solution such as aqueous monoethanol amine (MEA) is retained. In this absorber, nucleophilic amine functional groups in aqueous alkanolamine solution chemically absorb CO_2 from flue gas making bonds with carbon atom of CO_2. Depending on the types of applied amines in the absorber, the reaction product can be either carbamate or bicarbonate. The other part is a regenerator where heat is applied to cleave C-N bonds to regenerate aqueous alkanolamine solution and release CO_2. In the power plants adopting amine-based CCS system, significant amount of energy should be provided to regenerate amine sorbent resulting in sharp reduction of the plant's net efficiency and net electrical output. Approximately 55% of the CCS energy penalty is attributed to the heat consumed for the regeneration of amine sorbents.[21]

The considerable energy penalty of amine-based absorbents stems from their strong chemical bond with carbon atoms of CO_2. To optimize the interaction energy between sorbent and sorbate for ideal CO_2 capture and sorbent regeneration, solid adsorbents that are capable of physically adsorbing CO_2 have been suggested to be a more promising class of materials in CCS. Representative solid adsorbents proposed as CO_2 sorbents in CCS include zeolites, activated carbons, metal-organic frameworks (MOFs), and Porous Organic Polymers (POPs).

I. 3. Potential solid adsorbents for CO_2 capture: zeolite, activated carbon, metal organic frameworks

Zeolite is a class of porous crystalline aluminosilicates, whose structure is constructed with interlocking tetrahedra of SiO_4 and AlO_4 connected together through shared oxygen atoms in both various and well-regulated fashions. Negative charges dispersed throughout the frameworks due to substitution of AlO_4 tetrahedra for SiO_4 tetrahedra are compensated with exchangeable cations such as Na^+, K^+, Ca^{2+}, and Mg^{2+} which exist in the channels and cavities throughout the frameworks.[22] These charge balancing cations throughout the structures of zeolites are attributed to the dominant physisorption of CO_2 on zeolites. Carbon dioxide is physically adsorbed at a charge balancing cation by an ion-dipole interaction in a linear configuration and also chemisorbed in one or more bent configurations which are assumed to be carbonate ions formed by interaction with surface oxide ions adjacent to exchangeable cations.[23,24,25,26]

Activated carbons are a well-known class of materials which features mesoporous or microporous carbonaceous structures. Activated carbons can be generated with diverse but relatively inexpensive raw materials such as coals, industrial by-products, and wood or other biomass sources. Diversity in raw materials of activated carbon results in broad variety of pore size distribution, pore structure, and active surface structure allowing tailoring of their adsorptive properties. Activated carbons are prepared by two-steps which includes carbonization and activation. In carbonization step, raw materials of activated carbon release most of the non-carbon elements during a preliminary heating and pyrolysis of precursors in an inert atmosphere generating carbonaceous material, a rigid carbon skeleton with poor

surface properties. After carbonization step, carbonaceous material is activated by a physical or a chemical treatment producing suitable porosity and active sites, while increasing the surface area[27,28]

MOFs are a new class of crystalline porous materials which has attracted tremendous attention for the last two decades. MOFs are composed of metal-based nodes connected by organic ligands through strong coordination bonds constructing multidimensional coordination networks. Owing to their superb physical properties such as extraordinary surface areas, permanent porosities, and finely tunable pore surfaces to introduce suitable interaction energy with CO_2 molecules, MOFs have been suggested to be the most promising class of materials for selective CO_2 capture at large anthropogenic point sources.

I.4. Porous Organic Polymers

Porous Organic Polymers (POPs), an emerging class of microporous materials are constructed by covalent bonds of organic building blocks. POPs can be largely divided into crystalline POPs and amorphous POPs. Crystalline POPs with well-defined structures are prepared by crystallization of linked organic polymers into solid by using reversible and thermodynamically controlled organic reactions. Contrary to Crystalline POPs, amorphous POPs with structural defects are prepared by polymerization of organic building blocks using irreversible and kinetically controlled reactions.[29]

Yaghi and co-workers reported the first crystalline porous organic polymers, Covalent Organic Frameworks (COFs) (COF-1 and COF-5) in 2005.[30] COF-1 and COF-5 were synthesized by condensation reactions of phenyl diboronic acid $\{C_6H_4[B(OH)_2]_2\}$ and hexahyroxytriphenylene $[C_{18}H_6(OH)_6]$. As shown in Figure 2, COF-1 was synthesized by a dehydration reaction which allows three boronic acid molecules to converge to form a planar six-membered B_3O_3 (boroxine) ring liberating three water molecules. For the synthesis of COF-5, an analogous dehydration reaction, in which phenylboronic acid and 2,3,6,7,10,11-hexahydroxytriphenylene are condesned generating a five-membered BO2C2 ring, was used.

Powder x-ray diffraction (PXRD) analyses showed the crystalline structures of both COF-1 and COF-5 (figure 3). Porosity of COF-1 and COF-5 were confirmed by N_2 gas adsorption measurement at 77 K. from 0 to 1 bar. BET surface areas of COF-1 and COF-5 based on N_2 gas adsorption isotherms were 711 and 1590 $m^2\ g^{-1}$ respectively. The pore volumes of COF-1 and COF-5 at P/P_0 = 0.90 were 0.32 and 0.998 $cm^3\ g^{-1}$ respectivelty indicating permenant porosity of the materials.

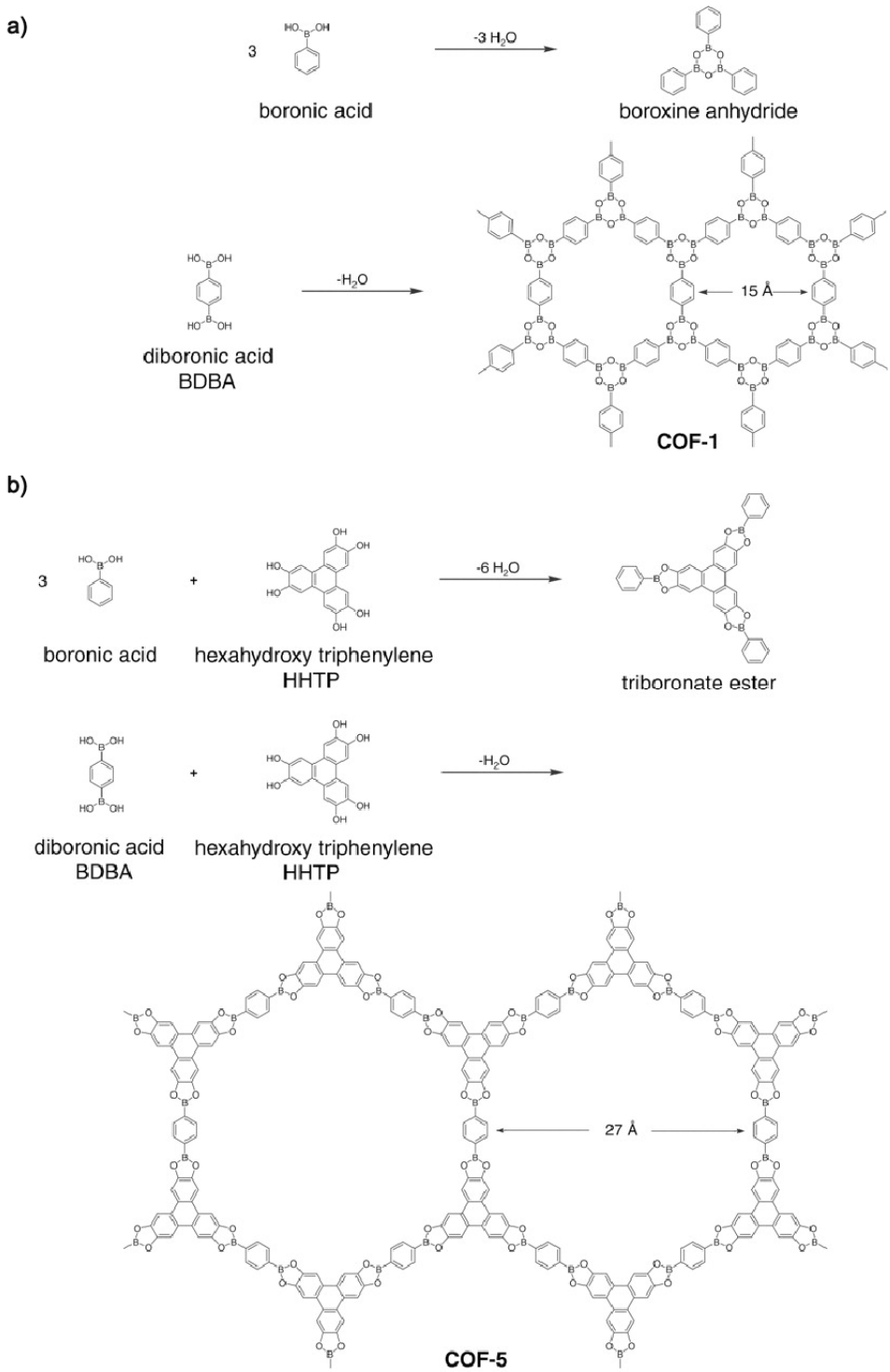

Figure 2. Synthetic schemes for the syntheses of a) COF-1 and b) COF-5

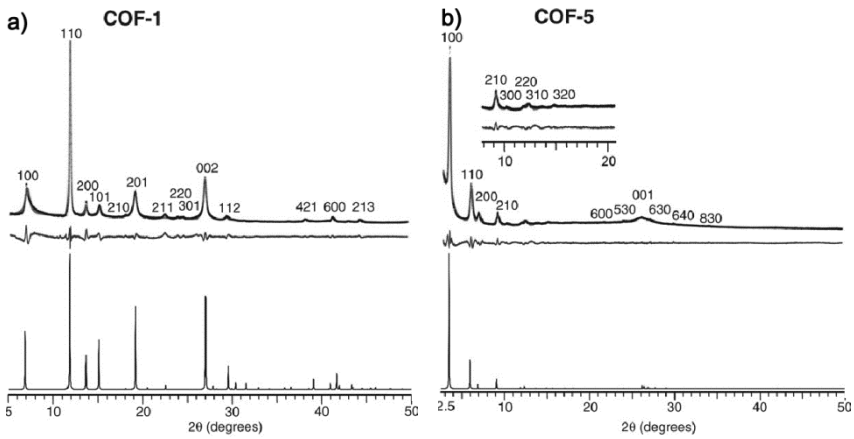

Figure 3. Powder x-ray diffraction analyses of a) COF-1 and b) COF-5. The bottom trace is the calculated PXRD pattern from *Cerius*.

Yaghi and co-workers expanded their research on COFs synthesizing 3D COFs with higher surface areas by adopting 3 D organic building block.[31] 3D COFs, COF-102 and COF-103 was synthesized by the same condensation reactions applied for the synthesis of COF-1 and COF-5. 3D organic building block, tetra(4-dihydroxyborylphenyl)methane (TBPM) was condensed resulting in COF-102 and co-condensation of TBPM and 2,3,6,7,10,11-hexahydroxytriphenylene resulted in COF-103. Ar isotherms of COF-103 and 103 were measured at 87 K from 0 to 760 torr and their BET surface areas were calculated based on the isotherms. Both COF-102 and COF-103 exhibited much higher surface areas (COF-102: 3472 m^2g^{-1} and COF-103: 4210 m^2g^{-1}) than the previously reported 2D COFs (COF-1 and COF-5).

Zhu and co-workers prepared a representative 3D amorphous porous organic polymer, Porous Aromatic Framework-1 (PAF-1).[5] Phenyl rings of a tetrahedral building unit, tetrakis(4-bromophenyl)methane were coupled using the nickel(0)-catalyzed Yamamoto-type Ullmann cross-coupling reaction. This reaction produced

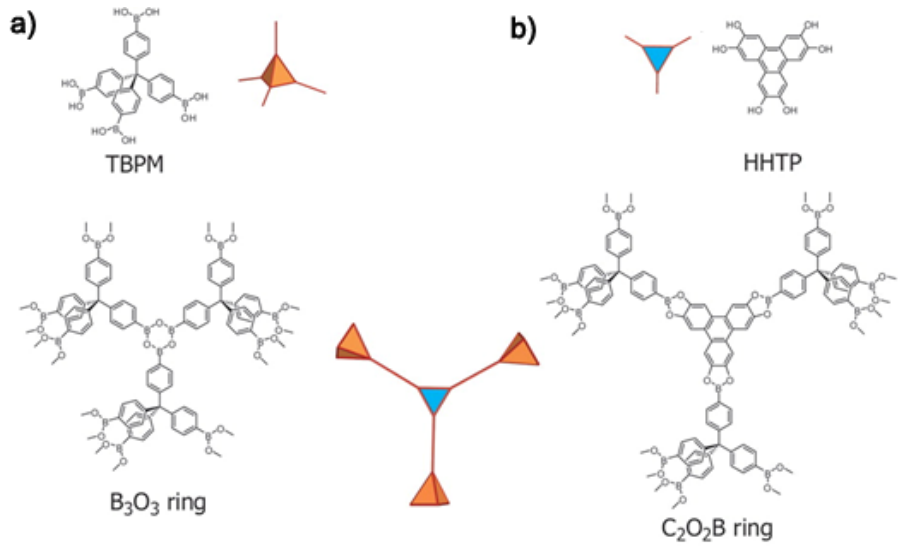

Figure 4. Representative condensation routes to 3D COFs. a) COF-102 and b) COF-103.

an offwhite powdered compound PAF-1, which has a low density and is not soluble in any common organic solvents. PAF-1 adsorbed high amount of N_2 (2000 cm^3g^{-1}) at 77 K from P/P_0 = 0 to P/P_0=0.94 giving an exceptionally high BET surface area (5600 m^2 g^{-1}). In addition to high surface area, PAF-5 displayed high thermal and chemical stability. PAF-1 was stable up to 520 ^oC in TGA analysis and stable in air and common organic solvents such as alcohols, THF, and DMF.

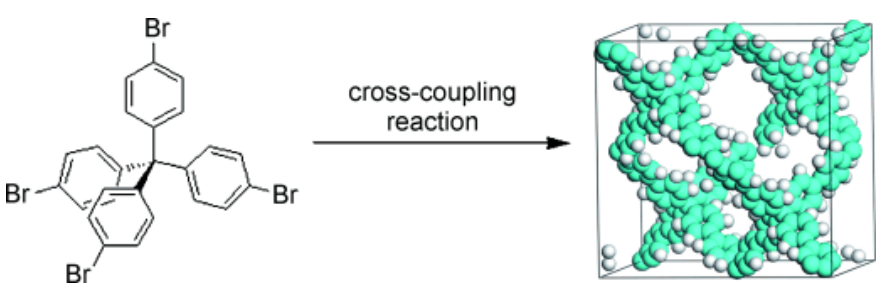

Figure 5. Syntetic scheme for the synthesis of PAF-1.

II. Experimental Section

General Methods. All chemicals and solvents used in the syntheses were of reagents grade and used without further purification. Branched polyethylenimine (PEI, Mw, ~800) was purchased from Sigma Aldrich. 1,3,5-tris(4-bromophenyl)benzene and PAF-5 were prepared by the methods previously reported.[11,32] Infrared spectra were recorded with a Perkin-Elmer Spectrum One FT-IR spectrophotometer. Thermogravimetric analyses (TGA) were carried out at a scan rate of 5 °C/min, using TGA Q50 of TA instruments. Elemental analyses were performed with a Perkin-Elmer 2400 Series II CHN analyzer.

Preparation of PAF-5 Impregnated with Polyethylenimine, PEI(x wt%)⊂PAF-5 (X= 10~40 wt%). PAF-5 was impregnated with a branched polyethylenimine (PEI, Mw, ~800) by a previously reported wet impregnation method.[33] Before PEI impregnation, as-synthesized PAF-5 was activated under reduced pressure at 373 K for 24 h. Various amounts of PEI was dissolved in anhydrous methanol (25 mL) by stirring for 10 min, and activated PAF-5 (*ca.* 0.2 g) was added to the solution. The PAF-5 slurry in the PEI/methanol solution was stirred and sonicated under each condition shown in Table 1. Finally, the resulting slurry was filtered, washed with anhydrous methanol (10 mL x 3), and activated at 373 K under reduced pressure for 24 h. The amount of PEI impregnated in PAF-5 was determined by TGA data as well as elemental analysis data (Table S2) after activating the as-synthesized PEI(x wt%)⊂PAF-5.

Table. 1. Conditions for impregnating various amounts of PEI in PAF-5 (*ca.* 0.2 g).

Compound	PEI (g)	stirring time (h) /temp (K	sonication time(h) /temp (K)	amount of impregnated PEI (wt%)
PEI(10 wt%)⊂PAF-5	1.0	-	1/298	10.4
PEI(30 wt%)⊂PAF-5	2.0	3/298	3/323	29.6
PEI(40 wt%)⊂PAF-5	3.0	6/298	6/323	39.7

Water Stability Test. The activated PEI(40 wt%)⊂PAF-5 (*ca.* 0.2 g) was exposed to water vapor in a closed glass bottle for 7 days at 313 K and then activated under reduced pressure at 373 K for 48 h.

Gas Cycling Experiment. Prior to gas cycling experiment, the sample was activated at 373 K under reduced pressure for 24 h. The activated sample was introduced to a thermogravimetric apparatus under N_2, and then the CO_2 gas cycling experiments were performed at 313 K on a TGA Q50 by using a stream of 15% (v/v) CO_2 in N_2 and a stream of 15% (v/v) CO_2 in He, followed by a stream of pure N_2. A flow rate of the gas was 60 mL/min.

Low Pressure Gas Sorption Measurements. The gas adsorption-desorption experiments were performed by using an automated micropore gas analyzer Autosorb-3B (Quantachrome Instruments). All gases used were of 99.9999% purity. Gas sorption isotherms for N_2 were monitored at 77, 298, 313, and 323 K, and CO_2 gas sorption isotherms were conducted at 298, 313, and 323 K at each equilibrium pressure by the static volumetric method. An exactly measured amount of the solid, which was activated at 373 K under reduced pressure, was introduced into the gas-sorption apparatus and the sample was reactivated at 373 K under high vacuum (10^{-4} atm) for 1 h. After each gas sorption measurement, the sample was precisely weighed again. From the N_2 gas isotherms at 77 K, surface area, pore size distribution, and

pore volume were calculated. Multipoint BET surface area was estimated by using the data recorded at P/P_0 = 0.005 - 0.1 atm. The pore size distribution and pore volume were calculated from non-local density functional theory (NLDFT) applying the model of carbon as an adsorbent and slit pore.

Calculation of Isosteric Heat of CO_2 Adsorption. Pressure as a function of the amount of adsorbed CO_2 was determined by fitting the adsorption isotherms measured at 298, 313, and 323 K to the dual-site Langmuir equation (eq 1). In eq 1, P is pressure (atm), N is the amount adsorbed gas (mmol g^{-1}), N_m is the amount of adsorbed gas at saturation, and b is a constant. The isosteric heat (Q_{st}) of the CO_2 adsorption was calculated by applying these fits to the Clausius-Clapeyron equation (eq 2).[34]

$$N = \frac{N_{m,A} b_A P}{1 + b_A P} + \frac{N_{m,B} b_B P}{1 + b_B P} \qquad (1)$$

$$\frac{\partial(\ln P)}{\partial(1/T)} = -\frac{Q_{st}}{R} \qquad (2)$$

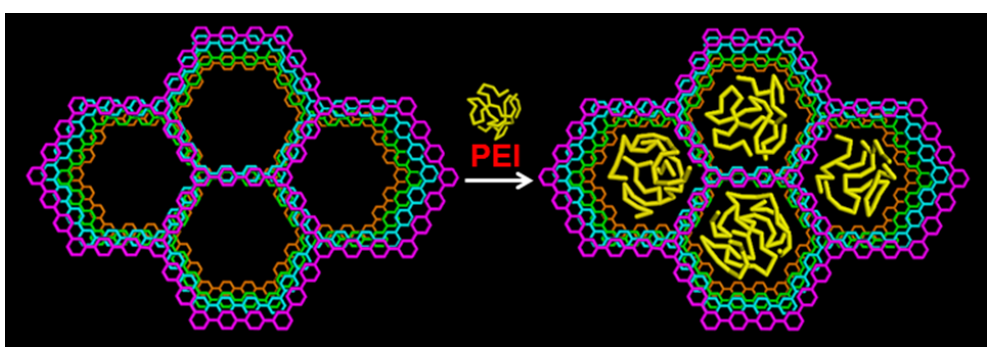

Figure 6. Schematic illustration of PEI impregnation in PAF-5

III. Results and Discussion

Characterization of impregnated PEI in PAF-5. The degree of PEI-impregnation in the 1D channels of PAF-5 was determined by thermogravimetric analyses (TGA) as shown in Figure 7. While dried PAF-5 was stable up to 873 K, PEI-impregnated PAF-5 adsorbents showed a sharp weight loss between 573 and 673 K, which is attributed to the thermal decomposition of PEI. The weight percent of PEI in PEI(x wt%)⊂PAF-5 (x= 10~40 wt%) was determined by measuring the degree of weight loss in this range.

The impregnation of PEI in the 1D channels of PAF-5 was further confirmed by FT-IR and elemental analyses. In the IR spectra (Figure 8), PEI-impregnated PAF-5 adsorbents showed a broad peak at around 3300 cm^{-1} which corresponds to the amine functional groups found in PEI. Due to hydrogen bonding between the amine groups in PEI, peak broadening occurred and identification of the respective peaks for the primary and secondary amines was not possible.

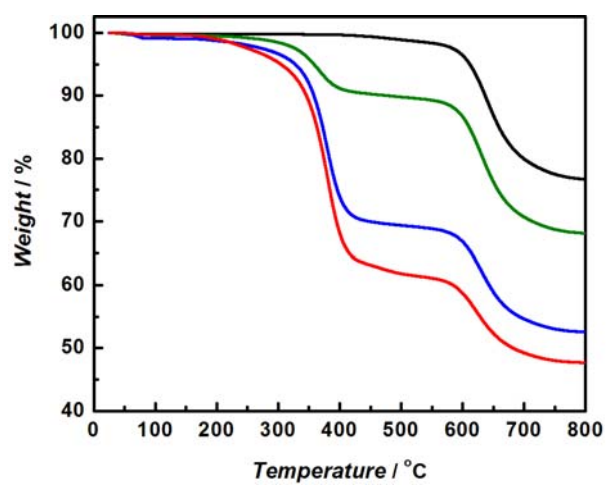

Figure 7. TGA traces for PAF-5 (black), PEI(10 wt%)⊂PAF-5 (green), PEI(30 wt%)⊂PAF-5 (blue), and PEI(40 wt%)⊂PAF-5 (red).

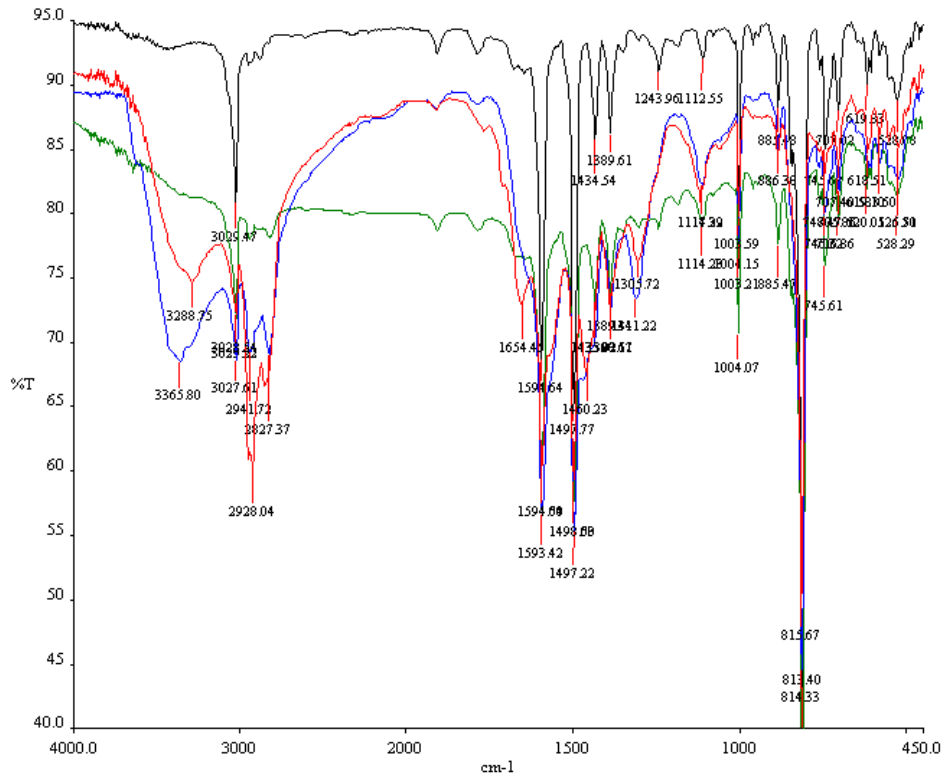

Figure 8. IR spectra of PAF-5 (black), PEI(10 wt%)⊂PAF-5 (green), PEI(30 wt%)⊂PAF-5 (blue), and PEI(40 wt%)⊂PAF-5 (red)

In the elemental analyses, the increase in weight percent of nitrogen was observed, as more PEI was incorporated into PAF-5. Sharp reduction in C/N ratios found in PEI(x wt%)⊂PAF-5 also indicated successful impregnation of PEI in PAF-5.

Surface areas and porosity of PAF-5 and PEI(x wt%)⊂PAF-5. To investigate the surface areas and porosity of pristine PAF-5 and PEI(x wt%)⊂PAF-5, the materials were activated by the heat-evacuation method (under reduced pressure at 373 K for 24 h), and N_2 adsorption and desorption isotherms of PAF-5 and PEI (x wt%)⊂PAF-5 were measured at 77 K. Pristine PAF-5 adsorbed *ca.* 1000 cc g^{-1} of N_2 at 0.9 atm giving a BET surface area of 2070 m^2g^{-1}. The pore size distribution and pore volume

Table 2. Elemental Analysis Data of PAF-5, PEI(10 wt%)⊂PAF-5, PEI(30 wt%)⊂PAF-5, and PEI(40 wt%)⊂PAF-5.[a]

Compound	C	N	H	C/N
PAF-5 ($C_{60}H_{36}$)	93.3(95.3)	0.24 (0.00)	5.02 (4.76)	
PEI(10 wt%)⊂PAF-5	89.4	2.76	5.58	37.8
PEI(30 wt%)⊂PAF-5	77.2	9.73	7.08	9.26
PEI(40 wt%)⊂PAF-5	72.9	11.7	8.68	7.27

[a]Calculated values are in the parentheses.

were also calculated from non-local density functional theory (NLDFT) applying the model of carbon as an adsorbent and slit pore. A large pore width of 2.11 nm and pore volume of 1.43 cc g^{-1} were determined from the NLDFT calculations. The values of BET surface area, pore width, and pore volume calculated in this work are slightly higher than those of previously reported PAF-5.[11]

We also applied the supercritical CO_2 drying method to activate PAF-5 and measured N_2 adsorption and desorption isotherms at 77 K. Based on the N_2 adsorption isotherm of PAF-5 activated by the supercritical CO_2 drying method, BET surface area (2150 m^2 g^{-1}), pore width (2.02 nm), and pore volume (1.34 cc g^{-1}) were calculated and found to be similar to those of PAF-5 activated by the heat-evacuation method. The high surface area as well as large pore width and volume of PAF-5 prove that PAF-5 is an appropriate host for PEI incorporation. As the weight percent of PEI in PAF-5 increases, a gradual decrease in N_2 uptake at 77 K was observed (Figure 10). The BET surface area of PEI(40 wt%)⊂PAF-5 wass reduced to 40.3 m^2 g^{-1} and its pore volume was also reduced to 0.046 cc g^{-1} indicating a complete saturation of PEI

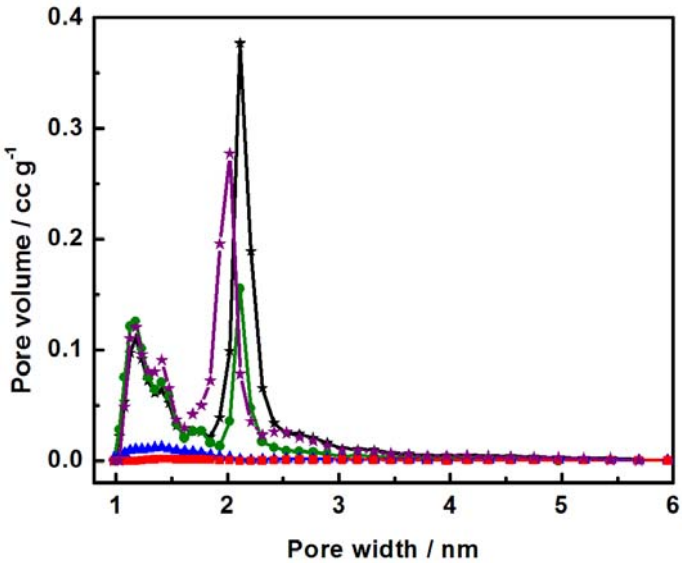

Figure 9. Pore width distributions of **PAF-5** (★), **PEI(10 wt%)⊂PAF-5** (●), **PEI(30 wt%)⊂PAF-5** (▲), and **PEI(40 wt%)⊂PAF-5** (■), calculated from non-local density functional theory (NLDFT) applying the model of carbon as an adsorbent and slit pore.

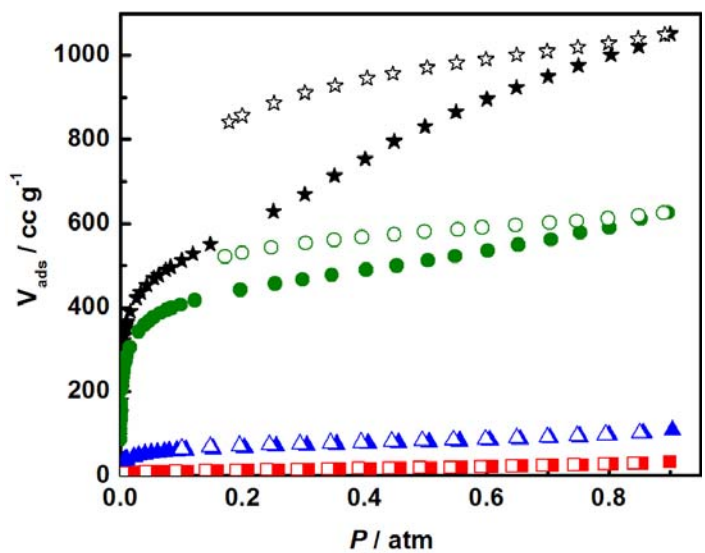

Figure 10. N_2 gas adsorption and desorption isotherms at 77 K. PAF-5 (★), PEI(10 wt%)⊂PAF-5 (●), PEI(30 wt%)⊂PAF-5 (▲), and PEI(40 wt%)⊂PAF-5 (■) activated by heat-evacuation method (under reduced pressure at 373 K for 24 h).

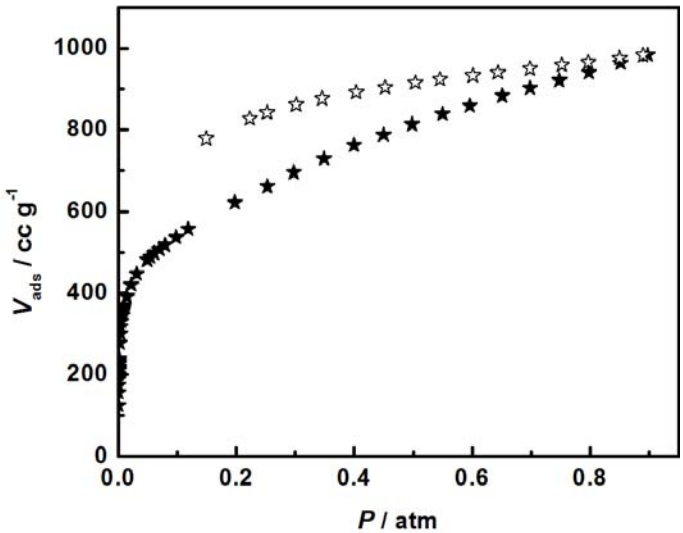

Figure 11. N_2 gas adsorption and desorption isotherms measured at 77 K: PAF-5 (★) activated by CO_2 supercritical drying method.

in the channels of PAF-5. It should be noted that C-H···π interaction between the methylene groups in PEI and phenyl rings of PAF-5 might contribute to stable PEI-impregnation into PAF-5.

Table 3. Surface areas and Porosity of PAF-5 and PEI(x wt%)⊂PAF-5

Compound	S_{BET} (m^2 g^{-1})[a]	V_{total} (cm^3 g^{-1})[a]
PAF-5	2070 (2150)	1.43 (1.34)
PEI(10 wt%)⊂PAF-5	1640	0.836
PEI(30 wt%)⊂PAF-5	233	0.152
PEI(40 wt%)⊂PAF-5	40.3	0.046

Gas sorption mesurement of PAF-5 and PEI(x wt%)⊂PAF-5. CO_2 adsorption and desorption isotherms of PAF-5 and PEI(x wt%)⊂PAF-5 were measured at 298, 313,

and 323 K up to 1 atm to evaluate the CO_2 uptake capacity of the PEI-impregnated PAF-5 adsorbents. As shown in Figure 12, pristine PAF-5 showed linearly increasing CO_2 adsorption isotherms uptaking 1.2, 0.8, and 0.7 wt% under 0.15 atm of CO_2 pressure at 298, 313, and 323 K. However, the CO_2 adsorption isotherms of PEI-loaded adsorbents changed to type-I isotherms at all three different temperatures, resulting in a drastic increase in CO_2 uptake capacities at 0.15 atm. In particular, PEI(40 wt%)⊂PAF-5 adsorbed 11.7 wt%, 11.1 wt%, and 10.9 wt% of CO_2 under 0.15 atm of CO_2 pressure at 298 K, 313 K, and 323 K, respectively, which are 10, 14, and 16 times greater than those of pristine PAF-5. The drastic increase in CO_2 uptake capacity at low CO_2 pressure stems from the strong interactions between the amine groups impregnated in PAF-5 and CO_2 molecule**s.**

N_2 adsorption and desorption isotherms of PAF-5 and PEI(x wt%)⊂PAF-5 were also measured up to 1 atm. Contrary to the CO_2 adsorption isotherms, PEI(x wt%)⊂PAF-5 showed a gradual reduction in N_2 uptake capacities at 298, 313, and 323 K as the weight percent of impregnated PEI in PAF-5 increased.

Table 4. Gas uptake capacities of PAF-5 and PEI(x wt%)⊂PAF-5

Compound	CO_2 uptake capacity (mmol g^{-1})[a]	N_2 uptake capacity (mmol g^{-1})[b]
PAF-5'	1.2/0.8/0.7	
PEI(10 wt%)⊂PAF-5	3.2/2.7/2.3	
PEI(30 wt%)⊂PAF-5	8.8/8.1/7.6	
PEI(40 wt%)⊂PAF-5	11.7/11.1/10.9	

[a]From the CO_2 gas isotherms measured at 298/313/323 K up to 0.15 atm. [b]From the N_2 gas isotherms measured at 298/313/323 K up to 0.85 atm.

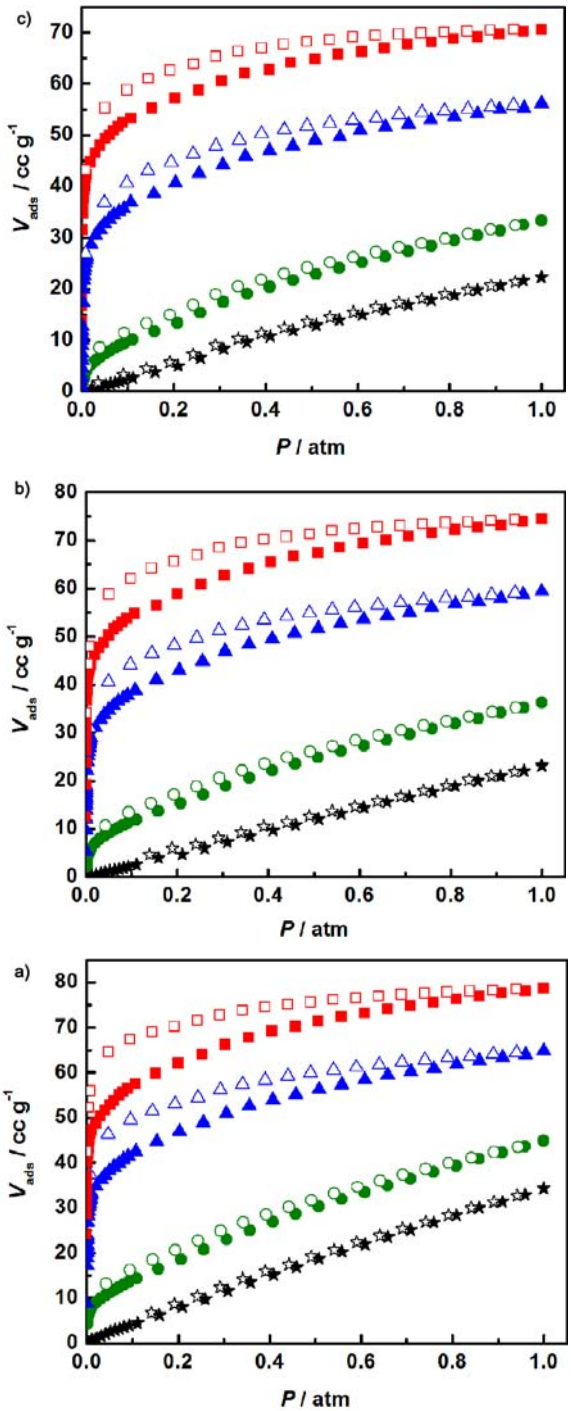

Figure 12. CO_2 gas adsorption and desorption isotherms measured at a) 298 K, b) 313 K, and c) 323 K. PAF-5 (★), PEI(10 wt%)⊂PAF-5 (●), PEI(30 wt%)⊂PAF-5 (▲), and PEI(40 wt%)⊂PAF-5 (■).

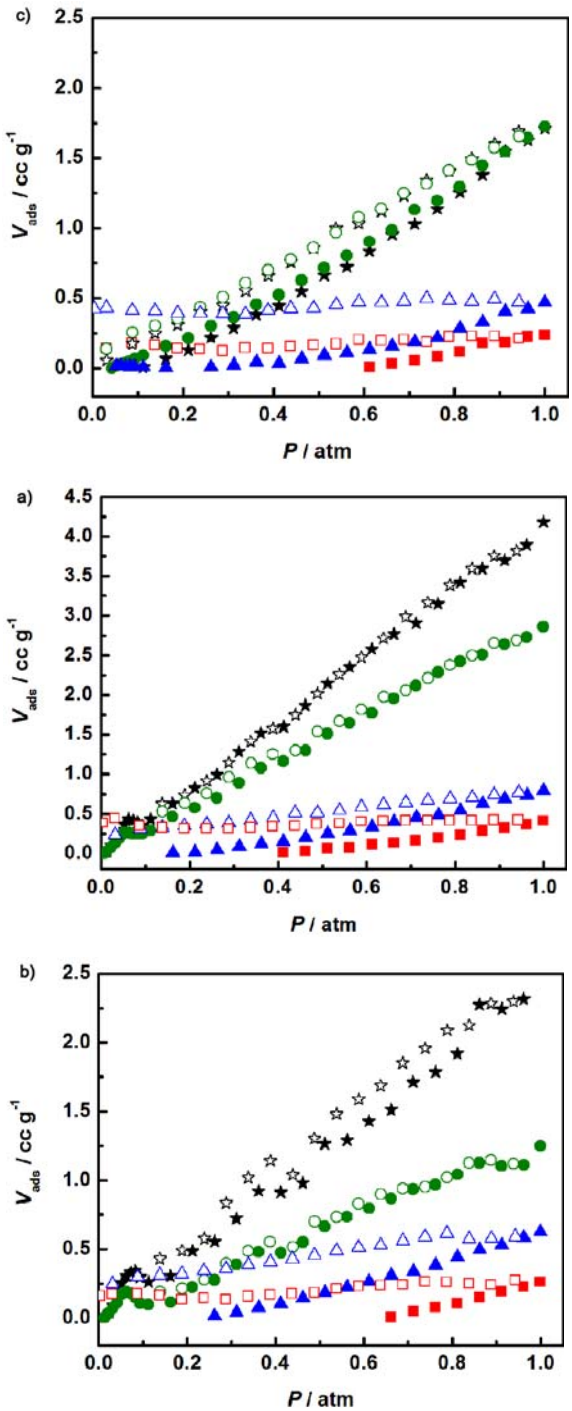

Figure 13. N_2 gas adsorption and desorption isotherms measured at a) 298 K, b) 313 K, and c) 323 K. PAF-5 (★), PEI(10 wt%)⊂PAF-5 (●), PEI(30 wt%)⊂PAF-5 (▲), and PEI(40 wt%)⊂PAF-5 (■).

Isosteric heat (Q_{st}) of the CO_2 adsorption in PAF-5 and PEI(x wt%)⊂PAF-5. Isosteric heat (Q_{st}) of the CO_2 adsorption in PAF-5 and PEI(x wt%)⊂PAF-5 were calculated by using Clausius-Clapeyron equation based on Dual-site Langmuir fit parameters obtained from the adsorption isotherms at 298, 313, and 323 K (Figure 15-18). The low coverage Q_{st} values of the CO_2 adsorption in a series of PEI-impregnated PAF-5 are 65.8~70.7 kJ mol^{-1}, which are remarkably higher than that (26.0 kJ mol^{-1}) of pristine PAF-5. The sharp increase in Q_{st} values of PEI-impregnated PAF-5 adsorbents are attributed to the strong interactions between the numerous amine functional groups of PEI and CO_2. The plot of Q_{st} values versus CO_2 uptake capacities shows two distinctive regions as shown in Figure 14. In particular, 30 wt% and 40 wt% PEI-loaded adsorbents display high Q_{st} values up to *ca.* 1.5 and 2.0 mmol g^{-1} of CO_2 loading, respectively. After the first region, Q_{st} values of both adsorbents are

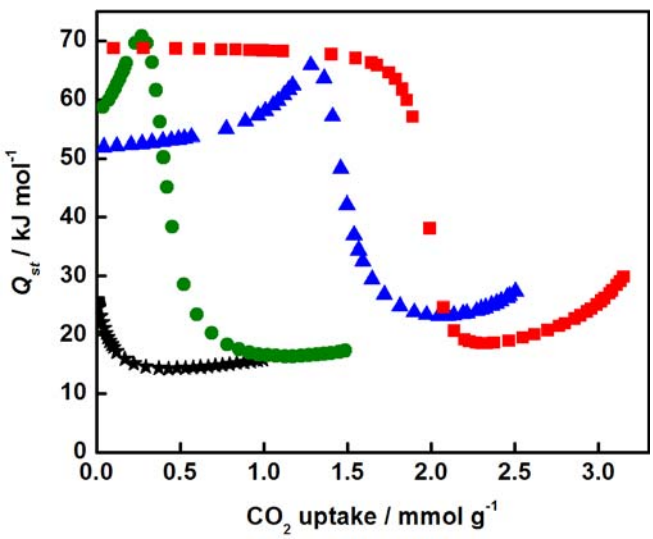

Figure 14. Isosteric heat of the CO_2 adosrption in PAF-5 and PEI(x wt%)⊂PAF-5. PAF-5 (★), PEI(10 wt%)⊂PAF-5 (●), PEI(30 wt%)⊂PAF-5 (▲), and PEI(40 wt%)⊂PAF-5 (■).

significantly decreased to low Q_{st} values. More interestingly, the first region of high Q_{st} values covers broader ranges of CO_2 uptake capacity as more amount of PEI is impregnated in PAF-5. This clearly shows that the amine functional groups in the impregnated PEI effectively interact with CO_2.

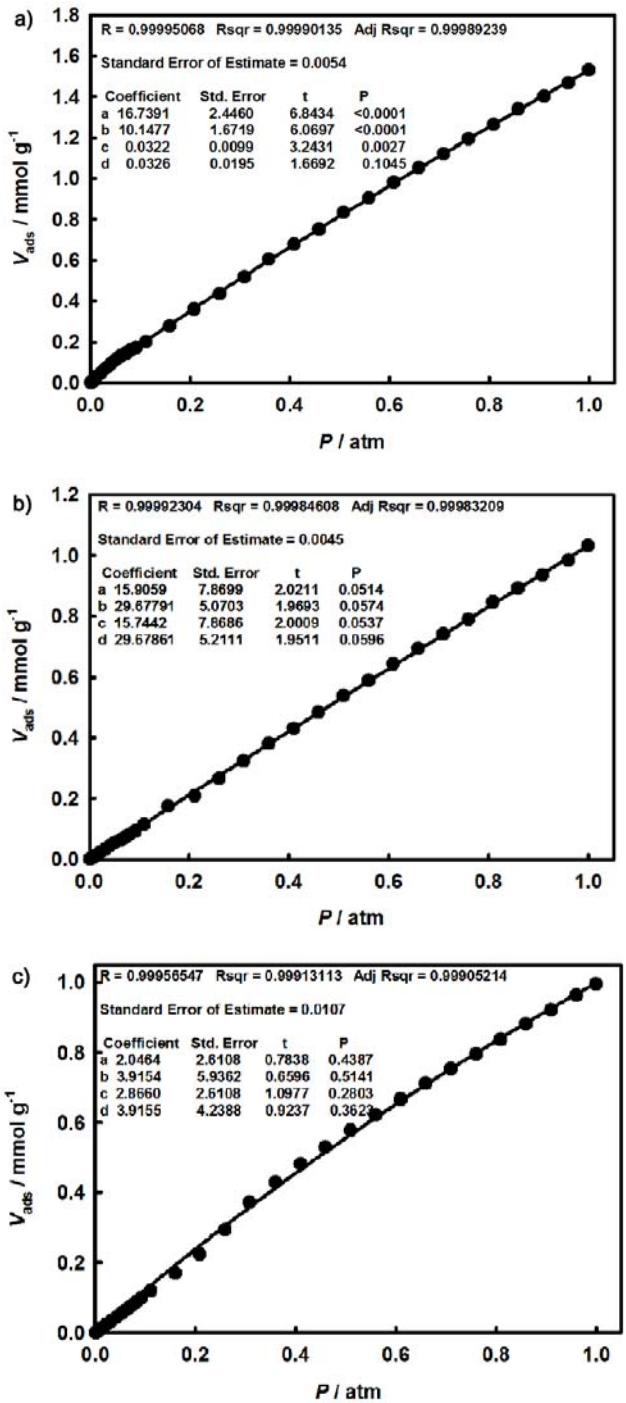

Figure 15. CO_2 gas adsorption isotherms of PAF-5 measured at a) 298 K, b) 313 K, and c) 323 K. The solid line corresponds to dual-site Langmuir equation fit.

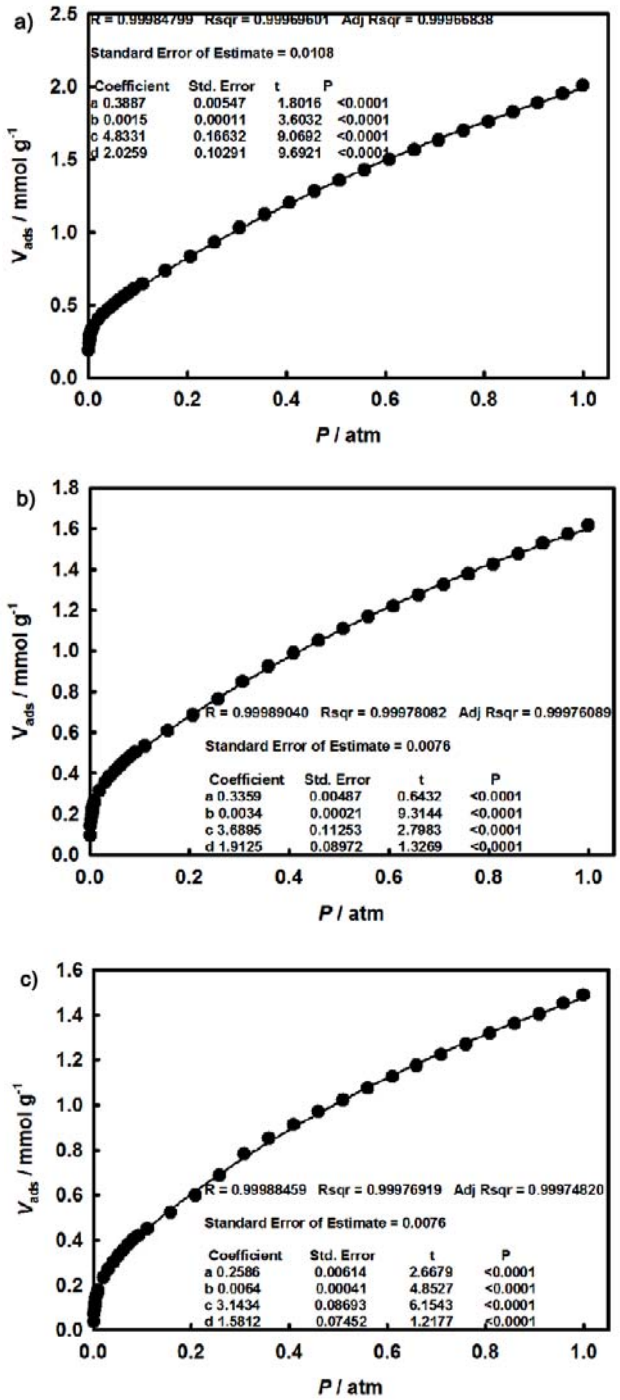

Figure 16. CO_2 gas adsorption isotherms of PEI(10 wt%)⊂PAF-5 measured at a) 298 K, b) 313 K, and c) 323 K. The solid line corresponds to dual-site Langmuir equation fit.

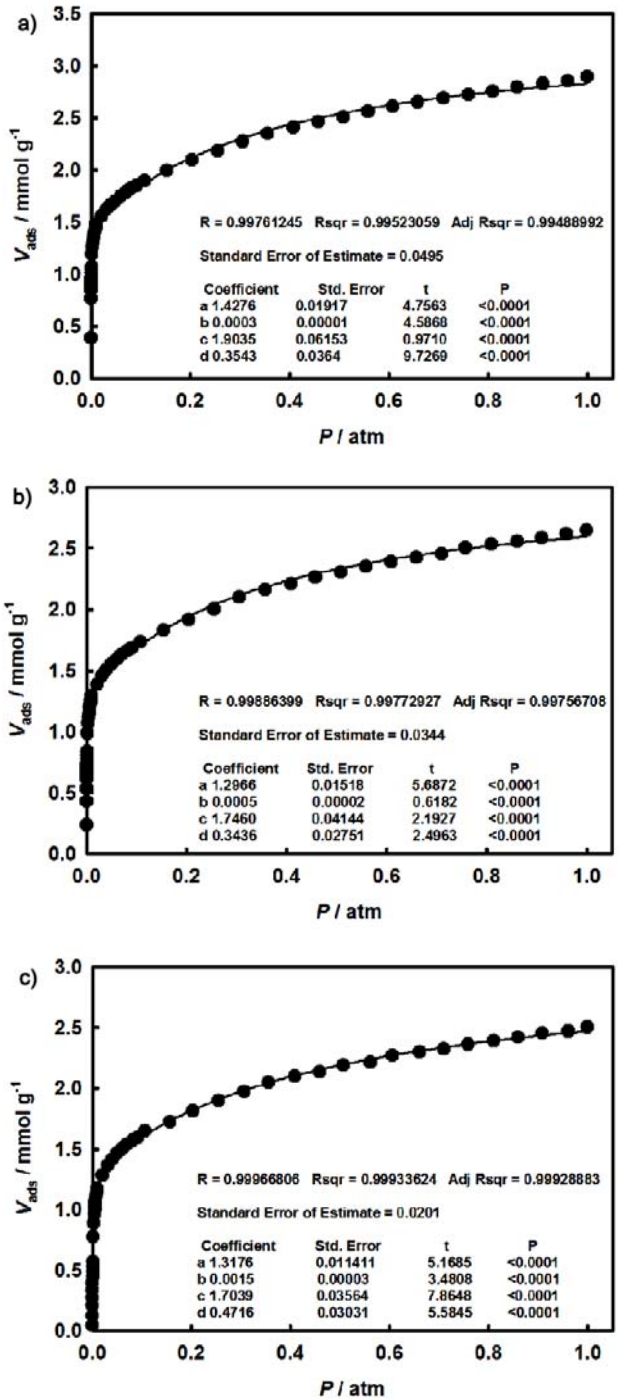

Figure 17. CO_2 gas adsorption isotherms of PEI(30 wt%)⊂PAF-5 measured at a) 298 K, b) 313 K, and c) 323 K. The solid line corresponds to dual-site Langmuir equation fit

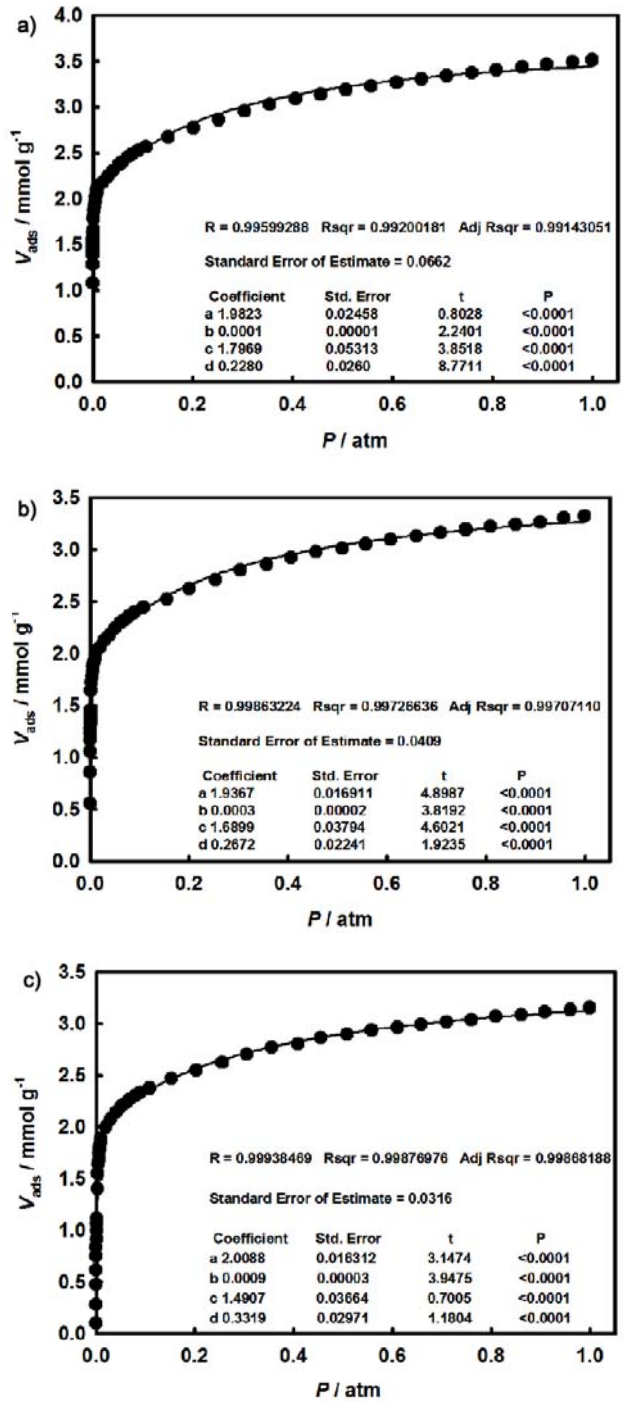

Figure 18. CO_2 gas adsorption isotherms of PEI(40 wt%)⊂PAF-5 measured at a) 298 K, b) 313 K, and c) 323 K. The solid line corresponds to dual-site Langmuir equation fit.

Selectivity for CO_2 adosrption over N_2 of PAF-5 and PEI(x wt%)⊂PAF-5. The CO_2 adsorption selectivity over N_2 was calculated on the single component adsorption isotherms of CO_2 and N_2 by using the molar ratio of the CO_2 uptake at 0.15 atm and the N_2 uptake at 0.85 atm at 298, 313, and 323 K. Selectivity based on IAST method could not be calculated since extremely low N_2 adsorption data for PEI-impregnated PAF-5 could not be reasonably fitted. A sharp increase in the CO_2 uptake at low CO_2 pressure and decrease in the N_2 uptake of the PEI-loaded PAF-5 adsorbents synergistically increase CO_2/N_2 selectivity at 298, 313, and 323 K. As shown in Table 5, PEI(40 wt%)⊂PAF-5 shows the highest selectivity (2160) at 313 K.

Table 5. Selectivity for CO_2 adsorption over $N_2$of PAF-5 and PEI(x wt%)⊂PAF-5 at 298, 313, and 323 K.

	Selectivity		
Compound	298 K	313 K	323 K
PAF-5	9.3	9.7	15.6
PEI(10 wt%)⊂PAF-5	37.3	74.4	45.9
PEI(30 wt%)⊂PAF-5	403	407	677
PEI(40 wt%)⊂PAF-5	1200	2160	1750

Gas cycling experiment of PAF-5 and PEI(x wt%)⊂PAF-5. To test possibility of the practical application of PEI-impregnated PAF-5 in post-combustion CO_2 capture, a gas cycling experiment was conducted by utilizing a thermogravimetric apparatus. For the adsorption process, the adsorbents were exposed to a stream of 15 % (v/v) CO_2 in

N_2 at 313 K, which approximately mimics flue gas. After the adsorption process, a pure N_2 stream was applied to regenerate the adsorbents at the elevated temperatures, at 313 K for PAF-5, at 323 K for PEI(10 wt%)⊂PAF-5, and at 343 K for PEI(30 wt%)⊂PAF-5 and PEI(40 wt%)⊂PAF-5. As shown in Figure 19, PAF-5 and PEI(10 wt%)⊂PAF-5 reached an equilibrium of CO_2 adsorption quickly, within 20 minutes, at 313 K. They showed relatively low CO_2 uptake capacities, 0.4 wt% and 1.9 wt%, respectively, and they were regenerated within 20 minutes under a N_2 flow at 313 and 323 K, respectively. Contrary to these, PEI(30 wt%)⊂PAF-5 and PEI(40 wt%)⊂PAF-5 adsorbed 8.4 wt% and 10.0 wt% of CO_2, respectively, at 313 K in 20 minutes, and they were completely regenerated within 20 minutes at 343 K, which is low desorption temperature, considering their very high Q_{st} values of the CO_2 adsorption. The 10.0 wt% weight increase of PEI(40 wt%)⊂PAF-5 in the gas cycling experiment is similar to 11.1 wt% CO_2 uptake at 0.15 atm in the CO_2 single component adsorption isotherm measured at 313 K. This 10.0 wt% of CO_2 uptake under a stream of 15% CO_2 in N_2 (v/v) at 313 K is one of the highest uptake capacities ever reported.

Previously reported PEI-decorated adsorbents such as PEI/Zr14-SBA-15[35], 65PEI/monolith[36], and PEI-MIL-101-125[37], or amine-functionalized adsorbent such as mmen-Mg_2(dobpdc)[38] suffered from a slow adsorption (12 h)[35] or desorption process (*ca.* 100 min),[36] in addition to a high energy penalty derived from a high regeneration temperature.[37,38] However, PEI(40 wt%)⊂PAF-5 adsorbs remarkably high amount of CO_2 and the material can be regenerated quickly at a slightly increased temperature (343 K). Furthermore, even after 10 adsorption/desorption cycles, the adsorbent shows neither material decomposition nor decrease of CO_2 uptake capacity (Figure 19).

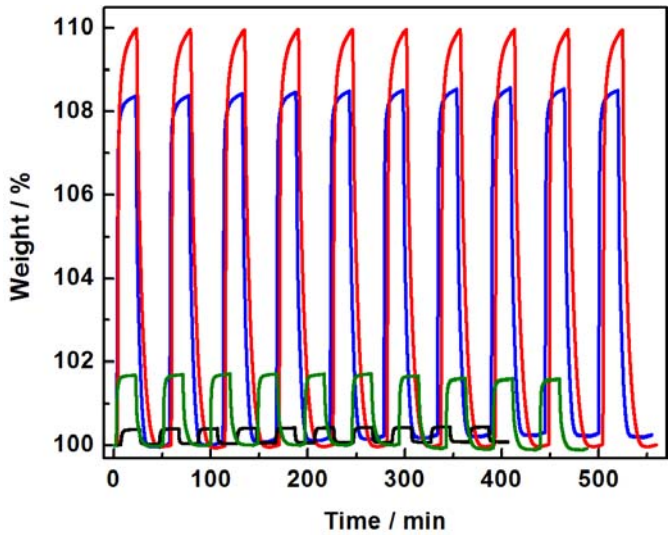

Figure 19. Gas cycling data of PAF-5 (black), PEI(10 wt%)⊂PAF-5 (green), PEI(30 wt%)⊂PAF-5 (blue), and PEI(40 wt%)⊂PAF-5 (red) with under the stream of 15 % CO_2 (v/v) in N_2 at 313 K followed by a pure N_2 stream at 343 K for PEI(30 wt%)⊂PAF-5 and PEI(40 wt%)⊂PAF-5, and at 323 K for PEI(10 wt%)⊂PAF-5. The adsorption and desorption time were given with 20 minutes in each process.

To validate the high selectivity of CO_2 adsorption over N_2 and to exclude the possibility of cooperative N_2 adsorption[39] in PEI(40 wt%)⊂PAF-5 under a CO_2/N_2 gas mixture, similar gas cycling experiments were performed by using a CO_2/He mixture since He cannot be adsorbed by any adsorbents. In the gas cycling experiment under the CO_2/He (15:85, v/v) gas mixture at 313 K, PEI(40 wt%)⊂PAF-5 increased its weight by 10.3 wt% within 20 minutes (Figure 20), similarly to 10.0 wt% increase under the CO_2/N_2 (15:85, v/v) gas mixture, and the material was completely regenerated under a N_2 stream at 353 K within 30 minutes. The results suggest that the material adsorbs only CO_2 under the CO_2/N_2 gas mixture.

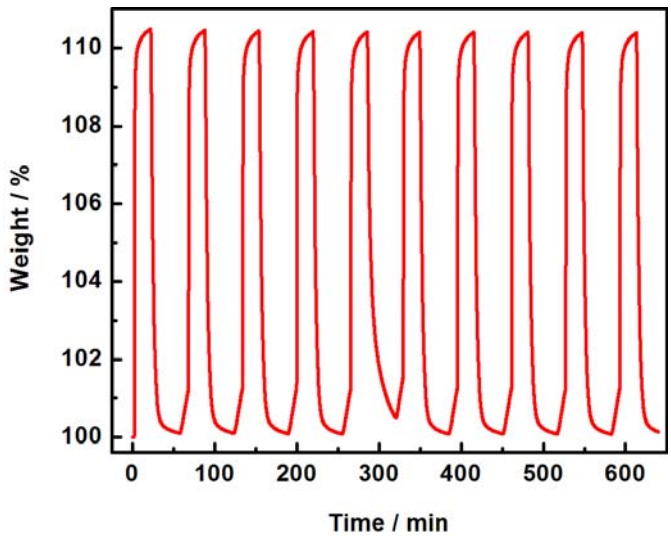

Figure 20. Gas cycling data of PEI(40 wt%)⊂PAF-5 under a flow of 15% CO_2 (v/v) in He at 313 K. The adsorption and desorption time were given 20 and 30 minutes respectively. For desorption process, temperature was elevated to 353 K under a N_2 flow.

Water stability test of PEI(40 wt%)⊂PAF-5. Since the industrial flue gas contains water vapor, CO_2 capture material should have high stability against water vapor. To evaluate the water stability of PEI(40 wt%)⊂PAF-5, the adsorbent was exposed to water vapor in a closed bottle for 7 days at 313 K and then activated under reduced pressure at 373 K for 48 hours. In thermogravimetric analyses, water-exposed PEI(40 wt%)⊂PAF-5 showed the same thermal decomposition pattern as the original sample that was not exposed to water vapor (Figure 21). Furthermore, in the gas cycling experiment carried out with CO_2/N_2 (15:85, v/v) mixture-gas stream at 313 K and under a pure N_2 gas stream at 343 K, water-exposed PEI(40 wt%)⊂PAF-5 showed the same weight changes, indicating the robustness of the material against water (Figure 22).

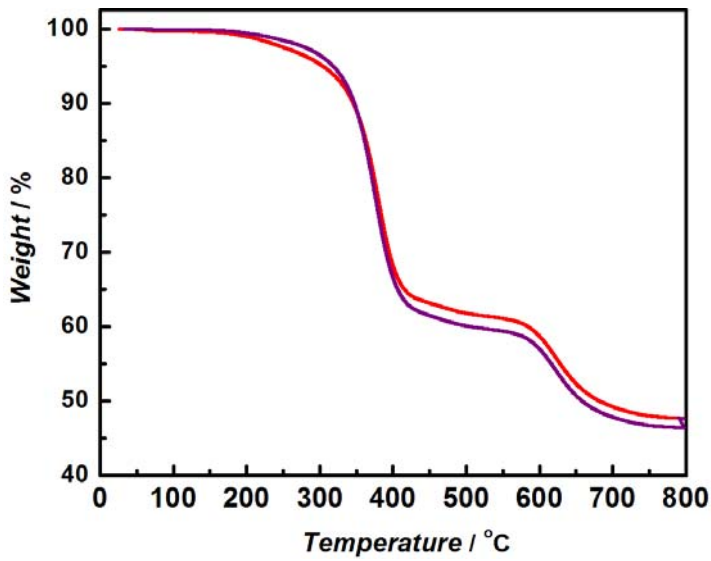

Figure 21. TGA traces for PEI(40 wt%)⊂PAF-5 a) before (red) and b) after (purple) exposure to water vapor at 313 K for 7 days.

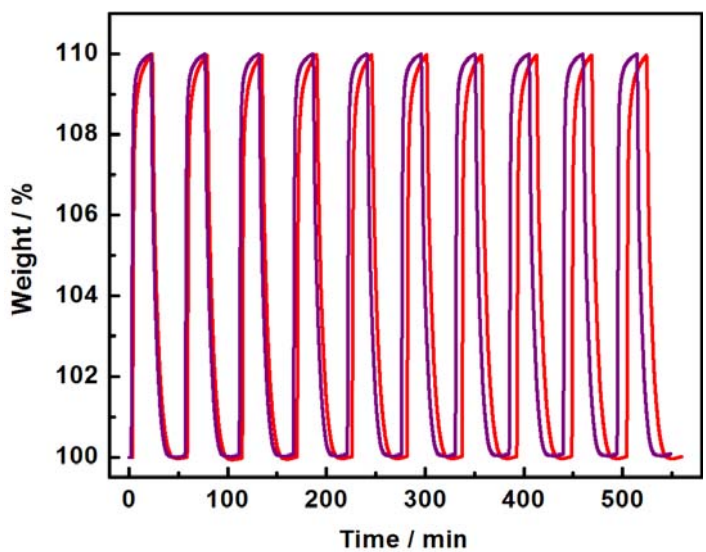

Figure 22. Gas cycling data of PEI(40 wt%)⊂PAF-5 and water vapor-exposed PEI(40 wt%)⊂PAF-5 (7 days at 313 K) under a flow of 15% CO_2 (v/v) in N_2 at 313 K. The adsorption and desorption time were given 20 minutes for each process. For desorption process, temperature was elevated to 343 K under a N_2 flow.

Working capacity of PEI(40 wt%)⊂PAF-5 in a temperature swing adsorption (TSA) process was calculated according to the equation, $\Delta N = N^{ads} - N^{des}$.[40] In the equation, N^{ads} is the amount of CO_2 adsorbed in the adsorption condition (under a flow of 15 % (v/v) CO_2 in N_2 at 313 K) and N^{des} is the amount of CO_2 adsorbed in the regeneration condition (under a pure CO_2 stream at regeneration temperature). To obtain the adsorbed amount of CO_2 at various regeneration temperature, we utilized the TGA apparatus. PEI(40 wt%)⊂PAF-5 first adsorbed CO_2 under a stream of 100% CO_2 at 313 K for 20 minutes (Figure 23). To regenerate the material under a 100% CO_2 stream, the temperature was elevated to 353, 393, and 403 K, respectively, till the equilibrium of weight change was reached at each temperature, and then the

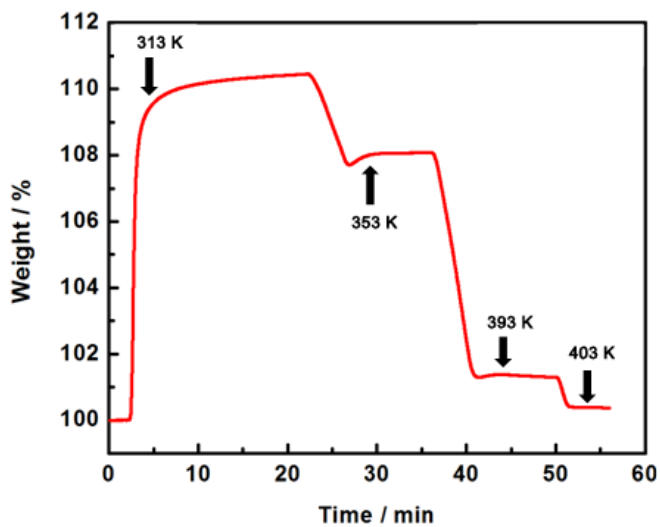

Figure 23. Temperature swing adsorption of **PEI(40 wt%)⊂PAF-5** measured by TGA apparatus. Adsorption process was conducted under a flow of 1 atm CO_2 at 313 K. After 20 minutes of adsorption process, temperature was raised to 353, 393, and 403 K with 10 minutes of equilibration time to regenerate the material under a flow of 1 atm CO_2.

temperature was maintained for another 10 minutes. The 10.0 wt% of CO_2 uptake was observed at 313 K, which was decreased to 7.8 wt% and then to 1.3 wt% as the temperature was elevated to 353 K and 393 K. Finally at 403 K, PEI(40 wt%)⊂PAF-5 released all the adsorbed CO_2 under the 100% CO_2 stream, displaying 10.0 wt% of working capacity (Figure 23).

IV. Conclusion

In conclusion, we have impregnated various amounts of PEI in a porous organic polymer (PAF-5) and demonstrated that the materials have high CO_2 gas uptake capacities, high isosteric heat of CO_2 adsorption, high selectivity for CO_2/N_2 adsorption, and high stability against water, and yet they need low energy penalty for regeneration of the adsorbents. As the amount of impregnated PEI increases, the CO_2 capture capability of the material becomes better. In particular, PEI(40 wt%)⊂PAF-5 shows 11.1 wt% of the CO_2 uptake capacity at 0.15 atm and 313 K, 68.7 kJ mol^{-1} of isosteric heat of the CO_2 adsorption, and 2160 of the CO_2/N_2 selectivity at low pressures. In a gas cycling experiment performed with a gas mixture of 15% (v/v) CO_2 in N_2 at 313 K, the adsorbent adsorbs 10.0 wt% of CO_2 in 20 minutes, which is one of the highest CO_2 uptake capacities at the given conditions. The material was regenerated within 20 minutes under a N_2 stream at 343 K, a much lower regeneration temperature than those (383 - 393 K) of the previously reported amine-functionalized adsorbents.[37,38] High thermal and water stability of the adsorbent were also verified by thermogravimetric analyses and gas cycling experiments after exposure to water vapor. To the best of our knowledge, this is the first PEI-impregnated porous organic polymer material that satisfies all criteria for effective post-combustion CO_2 capture, and it must be the promising CO_2 capture material for practical application.

References

1. Sumida, K.; Rogow, D. L.; Mason, J. A.; McDonald, T. M.; Bloch, E. D.; Herm, Z. R.; Bae, T.-H.; Long, J. R. *Chem. Rev.* **2012**, *112*, 724-781.
2. Park, H. J.; Suh, M. P. *Chem. Sci.* **2013**, *4*, 685-690.
3. Hong, D. H.; Suh, M. P. *Chem Commun* , **2012**, *48*, 9168-9170.
4. Choi, H.-S.; Suh, M. P. *Angew. Chem., Int. Ed.* **2009**, *48*, 6865-6869.
5. Ben, T.; Ren, H.; Ma, S.; Cao, D.; Lan, J.; Jing, X.; Wang, W.; Xu, J.; Deng, F.; Simmons, J. M.; Qiu, S.; Zhu, G. *Angew. Chem., Int. Ed.* **2009**, *48*, 9457-9460.
6. Xie, L.-H.; Suh, M. P. *Chem. -Eur. J.* **2013**, *19*, 11590-11597.
7. Islamoglu, T.; Gulam Rabbani, M.; El-Kaderi, H. M. *J. Mater. Chem. A* **2013**, *1*, 10259-10266.
8. Patel, H. A.; Je, S. H.; Park, J.; Chen, D. P.; Jung, Y.; Yavuz, C. T.; Coskun, A. *Nat. Commun.* **2013**, *4*, 1357.
9. Rabbani, M. G.; El-Kaderi, H. M. *Chem. Mater.* **2012**, *24*, 1511-1474.
10. Patel, H. A.; Karadas, F.; Byun, J.; Park, J.; Deniz, E.; Canlier, A.; Jung, Y.; Atilhan, M.; Yavuz, C. T. *Adv. Funct. Mater.* **2013**, *23*, 2270-2276.
11. Ren, H.; Ben, T.; Sun, F.; Guo, M.; Jing, X.; Ma, H.; Cai, K.; Qiu, S.; Zhu, G. *J. Mater. Chem.* **2011**, *21*, 10348-10353.
12. NOAA Mauna Loa dataset (reported online at: http://co2now.org/).
13. Solomon, S.; Plattner, G.-K.; Knutti, R.; Friedlingstein, P. *Proc. Natl. Acad. Sci.* **2009**, *106*, 1704-1709.

14. http://www.netl.doe.gov/technologies/carbon_seq/refshelf/2011_Sequestration_Program_Plan.pdf.

15. House, K. Z.; Harvey, C. F.; Aziz, M. J.; Schrag, D. P. *Energy & Environmental Science*, **2009**, *2*, 193-205.

16. Haszeldine, R. S.; *Science*, **2009**, *325*, 1647-1652.

17. Figueroa, J. D.; Fout, T.; Plasynski, S.; McIlvried, H.; Srivastava, R. D. *International Journal of Greenhouse Gas Control*, **2008**, *2*, 9-20.

18. Agarwal, A.; Biegler, L. T.; Zitney, S. E.; *Ind. Eng. Chem. Res.* **2010**, *49*, 5066-5079.

19. Plasynski, S. I.; Litynski, J. T.; McIlvried, H. G.; Srivastava, R. D. *Critical Reviews in Plant Science*, **2009**, *28*,123-138.

20. Buhre, B. J. P.; Elliott, L. K.; Sheng, C. D.; Gupta, R. P.; Wall, T. F.; *Progress in Energy and Combustion Science*, **2005**, *31***,** 283–307.

21. Echeverri, D. P.; Hoppock, D. C.; *Environ. Sci. Technol*, **2012**, *46*, 1243-1252.

22. Wang, Q. A.; Luo, J. Z.; Zhong, Z. Y.; Borgna, A. *Energy & Environmental Science*, **2011**, *4*, 42-55.

23. Bertsch, L.; Habgood, H. W. *J. Phys. Chem.*, **1963**, *67*, 1621-&.

24. Ward, J. W.; Habgood, H. W. *J. Phys. Chem.*, **1966**, *70*, 1178-&.

25. Walton, K. S.; Abney, M. B.; LeVan, M. D. *Microporous Mesoporous Mater.*, **2006**, *91*, 78-84.

26. Cavenati, S.; Grande, C. A.; Rodrigues, A. E. *J. Chem. Eng. Data*, **2004**, *49*, 1095-1101.

27. Choi, S.; Drese, J. H.; Jones, C. W. *Chemsuschem*, **2009**, *2*, 796-854.

28. Siriwardane, R. V.; Shen, M. S.; Fisher, E. P.; Poston, J. A. *Energy F uels*, **2001**, *15*, 279-284.

29. Xiao, F.; Xuesong, D.; Donglin, Jiang. *Chem. Soc. Rev.*, **2012**, *41*, 6010 -6022.

30. Cote, A. P.; Benin, A. I.; Ockwig, N. W.; O'Keeffe, M.; Matzger, A. J.; Yaghi, O. M. *Science*, **2005**, *310*, 1166-1170.

31. El-Kaderi, H. M.; Hunt, J. R.; Mendoza-Cortes, J. L.; Cote, A. P.; Ta ylor, R. E.; O'Keeffe M.; Yaghi, O. M. *Science*, **2007**, *316*, 268-272.

32. Zhao, Y.; Li, J.; Li, C.; Yin, K.; Ye, D.; Jia, X. *Green. Chem.* **2010**, *12*, 1370-1372.

33. Xu, X.; Song, C.; Andresen, J. M.; Miller, B. G.; Scaroni, A. W. *Ene rgy Fuels*, **2002**, *16*, 1463-1469.

34. Czepirski, L.; Jagiello, J.; *Chem. Eng. Sci.* **1989**, *44*, 797-801.

35. Kuwahara, Y.; Kang, D.-Y.; Copeland, J. R.; Brunelli, N. A.; Didas, S. A.; Bollini, P.; Sievers, C.; Kamegawa, T.; Yamashita, H.; Jones, C. W. *J. Am. Chem. Soc.* **2012**, *134*, 10757-10760.

36. Chen, C.; Yang, S.-T.; Ahn, W.-S.; Ryoo, R. *Chem. Commun.* **2009**, *3* 627-3629.

37. Lin, Y.; Yan, Q.; Kong, C.; Chen, L. *Sci. Rep.* **2013**, *3*, 1859.

38. McDonald, T. M.; Lee, W. R.; Mason, J. A.; Wiers, B. M.; Hong, C. S.; Long, J. R. *J. Am. Chem. Soc.* **2012**, *134*, 7056-7065.

39. D'Alessandro, D. M.; Smit, B.; Long, J. R. *Angew. Chem., Int. Ed.* **20 10**, *49*, 6058-6082.

40. Bae, Y. S.; Snurr, R. Q. *Angew. Chem., Int. Ed.* **2011**, *50*, 11586-115 96.

Supporting Information

Table S1. N_2 adsorption and desorption data at 77 K.

PAF-5		PEI (10 wt%)⊂PAF-5		PEI (30 wt%)⊂PAF-5		PEI (40 wt%)⊂PAF-5	
P **(atm)**	***V*** **(cc/g)**	***P*** **(atm)**	***V*** **(cc/g)**	***P*** **(atm)**	***V*** **(cc/g)**	***P*** **(atm)**	***V*** **(cc/g)**
1.26E-02	2.21E-02	4.32E-03	6.00E-04	1.62E-01	6.80E-03	4.12E-01	6.00E-03
2.26E-02	9.92E-02	5.02E-03	9.00E-04	2.12E-01	1.59E-02	4.62E-01	2.68E-02
3.24E-02	1.72E-01	6.04E-03	2.10E-03	2.62E-01	4.54E-02	5.12E-01	6.07E-02
4.22E-02	2.53E-01	7.01E-03	2.90E-03	3.12E-01	8.20E-02	5.62E-01	7.38E-02
5.20E-02	3.62E-01	9.24E-03	8.40E-03	3.62E-01	1.23E-01	6.12E-01	1.11E-01
6.21E-02	4.33E-01	9.85E-03	8.20E-03	4.12E-01	1.50E-01	6.62E-01	1.32E-01
7.23E-02	4.18E-01	1.27E-02	2.57E-02	4.62E-01	2.02E-01	7.12E-01	1.66E-01
8.26E-02	3.91E-01	2.25E-02	7.77E-02	5.12E-01	2.50E-01	7.62E-01	2.02E-01
9.30E-02	3.49E-01	3.23E-02	1.34E-01	5.62E-01	2.82E-01	8.12E-01	2.28E-01
1.12E-01	4.32E-01	4.23E-02	2.02E-01	6.12E-01	3.32E-01	8.62E-01	2.83E-01
1.62E-01	6.31E-01	5.20E-02	2.64E-01	6.62E-01	3.99E-01	9.12E-01	3.24E-01
2.12E-01	8.28E-01	6.24E-02	2.59E-01	7.12E-01	4.53E-01	9.62E-01	3.64E-01
2.62E-01	9.91E-01	7.26E-02	2.45E-01	7.62E-01	4.88E-01	9.99E-01	4.09E-01
3.11E-01	1.28E+00	8.28E-02	2.44E-01	8.12E-01	5.40E-01	9.42E-01	4.18E-01
3.61E-01	1.52E+00	9.30E-02	2.48E-01	8.62E-01	6.29E-01	8.88E-01	4.19E-01
4.12E-01	1.60E+00	1.12E-01	2.87E-01	9.12E-01	6.92E-01	8.38E-01	4.12E-01
4.62E-01	1.87E+00	1.61E-01	4.65E-01	9.62E-01	7.31E-01	7.88E-01	4.11E-01
5.11E-01	2.14E+00	2.12E-01	5.75E-01	9.99E-01	7.88E-01	7.38E-01	4.14E-01
5.61E-01	2.35E+00	2.62E-01	7.00E-01	9.43E-01	7.66E-01	6.88E-01	4.12E-01
6.12E-01	2.58E+00	3.12E-01	8.92E-01	8.88E-01	7.42E-01	6.38E-01	4.07E-01
6.61E-01	2.77E+00	3.61E-01	1.08E+00	8.38E-01	7.02E-01	5.88E-01	4.03E-01
7.11E-01	2.91E+00	4.12E-01	1.16E+00	7.88E-01	6.88E-01	5.38E-01	3.81E-01
7.61E-01	3.15E+00	4.62E-01	1.30E+00	7.38E-01	6.69E-01	4.88E-01	3.68E-01
8.11E-01	3.42E+00	5.11E-01	1.51E+00	6.88E-01	6.38E-01	4.38E-01	3.50E-01
8.61E-01	3.59E+00	5.61E-01	1.65E+00	6.38E-01	6.13E-01	3.88E-01	3.42E-01
9.12E-01	3.70E+00	6.12E-01	1.77E+00	5.88E-01	5.88E-01	3.38E-01	3.29E-01
9.61E-01	3.90E+00	6.61E-01	1.96E+00	5.38E-01	5.40E-01	2.88E-01	3.10E-01
9.99E-01	4.18E+00	7.11E-01	2.12E+00	4.88E-01	5.13E-01	2.38E-01	3.14E-01
9.39E-01	3.81E+00	7.62E-01	2.29E+00	4.38E-01	5.16E-01	1.88E-01	3.14E-01
8.88E-01	3.75E+00	8.11E-01	2.42E+00	3.88E-01	4.48E-01	1.38E-01	3.30E-01
8.38E-01	3.59E+00	8.61E-01	2.51E+00	3.38E-01	4.18E-01	8.80E-02	3.46E-01
7.88E-01	3.38E+00	9.12E-01	2.64E+00	2.88E-01	3.84E-01	3.11E-02	4.42E-01
7.38E-01	3.16E+00	9.62E-01	2.73E+00	2.38E-01	3.72E-01	3.97E-03	3.87E-01
6.88E-01	2.99E+00	9.99E-01	2.86E+00	1.88E-01	3.48E-01		
6.38E-01	2.71E+00	9.39E-01	2.69E+00	1.38E-01	3.29E-01		
5.88E-01	2.47E+00	8.88E-01	2.65E+00	8.81E-02	3.06E-01		
5.38E-01	2.26E+00	8.38E-01	2.50E+00	3.15E-02	2.33E-01		

4.88E-01	2.02E+00	7.88E-01	2.37E+00
4.39E-01	1.75E+00	7.39E-01	2.21E+00
3.88E-01	1.57E+00	6.88E-01	2.06E+00
3.38E-01	1.41E+00	6.39E-01	1.98E+00
2.89E-01	1.15E+00	5.88E-01	1.81E+00
2.39E-01	9.15E-01	5.38E-01	1.67E+00
1.89E-01	7.37E-01	4.89E-01	1.54E+00
1.38E-01	6.29E-01	4.40E-01	1.30E+00
		3.88E-01	1.26E+00
		3.39E-01	1.14E+00
		2.89E-01	9.61E-01
		2.39E-01	7.57E-01
		1.89E-01	6.33E-01
		1.38E-01	5.29E-01

Table S2. N_2 adsorption and desorption data at 298 K.

PAF-5		PEI (10 wt%)⊂PAF-5		PEI (30 wt%)⊂PAF-5		PEI (40 wt%)⊂PAF-5	
P **(atm)**	***V*** **(cc/g)**	***P*** **(atm)**	***V*** **(cc/g)**	***P*** **(atm)**	***V*** **(cc/g)**	***P*** **(atm)**	***V*** **(cc/g)**
1.26E-02	2.21E-02	4.32E-03	6.00E-04	1.62E-01	6.80E-03	4.12E-01	6.00E-03
2.26E-02	9.92E-02	5.02E-03	9.00E-04	2.12E-01	1.59E-02	4.62E-01	2.68E-02
3.24E-02	1.72E-01	6.04E-03	2.10E-03	2.62E-01	4.54E-02	5.12E-01	6.07E-02
4.22E-02	2.53E-01	7.01E-03	2.90E-03	3.12E-01	8.20E-02	5.62E-01	7.38E-02
5.20E-02	3.62E-01	9.24E-03	8.40E-03	3.62E-01	1.23E-01	6.12E-01	1.11E-01
6.21E-02	4.33E-01	9.85E-03	8.20E-03	4.12E-01	1.50E-01	6.62E-01	1.32E-01
7.23E-02	4.18E-01	1.27E-02	2.57E-02	4.62E-01	2.02E-01	7.12E-01	1.66E-01
8.26E-02	3.91E-01	2.25E-02	7.77E-02	5.12E-01	2.50E-01	7.62E-01	2.02E-01
9.30E-02	3.49E-01	3.23E-02	1.34E-01	5.62E-01	2.82E-01	8.12E-01	2.28E-01
1.12E-01	4.32E-01	4.23E-02	2.02E-01	6.12E-01	3.32E-01	8.62E-01	2.83E-01
1.62E-01	6.31E-01	5.20E-02	2.64E-01	6.62E-01	3.99E-01	9.12E-01	3.24E-01
2.12E-01	8.28E-01	6.24E-02	2.59E-01	7.12E-01	4.53E-01	9.62E-01	3.64E-01
2.62E-01	9.91E-01	7.26E-02	2.45E-01	7.62E-01	4.88E-01	9.99E-01	4.09E-01
3.11E-01	1.28E+00	8.28E-02	2.44E-01	8.12E-01	5.40E-01	9.42E-01	4.18E-01
3.61E-01	1.52E+00	9.30E-02	2.48E-01	8.62E-01	6.29E-01	8.88E-01	4.19E-01
4.12E-01	1.60E+00	1.12E-01	2.87E-01	9.12E-01	6.92E-01	8.38E-01	4.12E-01
4.62E-01	1.87E+00	1.61E-01	4.65E-01	9.62E-01	7.31E-01	7.88E-01	4.11E-01
5.11E-01	2.14E+00	2.12E-01	5.75E-01	9.99E-01	7.88E-01	7.38E-01	4.14E-01
5.61E-01	2.35E+00	2.62E-01	7.00E-01	9.43E-01	7.66E-01	6.88E-01	4.12E-01
6.12E-01	2.58E+00	3.12E-01	8.92E-01	8.88E-01	7.42E-01	6.38E-01	4.07E-01
6.61E-01	2.77E+00	3.61E-01	1.08E+00	8.38E-01	7.02E-01	5.88E-01	4.03E-01
7.11E-01	2.91E+00	4.12E-01	1.16E+00	7.88E-01	6.88E-01	5.38E-01	3.81E-01
7.61E-01	3.15E+00	4.62E-01	1.30E+00	7.38E-01	6.69E-01	4.88E-01	3.68E-01
8.11E-01	3.42E+00	5.11E-01	1.51E+00	6.88E-01	6.38E-01	4.38E-01	3.50E-01
8.61E-01	3.59E+00	5.61E-01	1.65E+00	6.38E-01	6.13E-01	3.88E-01	3.42E-01
9.12E-01	3.70E+00	6.12E-01	1.77E+00	5.88E-01	5.88E-01	3.38E-01	3.29E-01
9.61E-01	3.90E+00	6.61E-01	1.96E+00	5.38E-01	5.40E-01	2.88E-01	3.10E-01
9.99E-01	4.18E+00	7.11E-01	2.12E+00	4.88E-01	5.13E-01	2.38E-01	3.14E-01
9.39E-01	3.81E+00	7.62E-01	2.29E+00	4.38E-01	5.16E-01	1.88E-01	3.14E-01
8.88E-01	3.75E+00	8.11E-01	2.42E+00	3.88E-01	4.48E-01	1.38E-01	3.30E-01
8.38E-01	3.59E+00	8.61E-01	2.51E+00	3.38E-01	4.18E-01	8.80E-02	3.46E-01
7.88E-01	3.38E+00	9.12E-01	2.64E+00	2.88E-01	3.84E-01	3.11E-02	4.42E-01
7.38E-01	3.16E+00	9.62E-01	2.73E+00	2.38E-01	3.72E-01	3.97E-03	3.87E-01
6.88E-01	2.99E+00	9.99E-01	2.86E+00	1.88E-01	3.48E-01		
6.38E-01	2.71E+00	9.39E-01	2.69E+00	1.38E-01	3.29E-01		
5.88E-01	2.47E+00	8.88E-01	2.65E+00	8.81E-02	3.06E-01		
5.38E-01	2.26E+00	8.38E-01	2.50E+00	3.15E-02	2.33E-01		

4.88E-01	2.02E+00	7.88E-01	2.37E+00
4.39E-01	1.75E+00	7.39E-01	2.21E+00
3.88E-01	1.57E+00	6.88E-01	2.06E+00
3.38E-01	1.41E+00	6.39E-01	1.98E+00
2.89E-01	1.15E+00	5.88E-01	1.81E+00
2.39E-01	9.15E-01	5.38E-01	1.67E+00
1.89E-01	7.37E-01	4.89E-01	1.54E+00
1.38E-01	6.29E-01	4.40E-01	1.30E+00
		3.88E-01	1.26E+00
		3.39E-01	1.14E+00
		2.89E-01	9.61E-01
		2.39E-01	7.57E-01
		1.89E-01	6.33E-01
		1.38E-01	5.29E-01

Table S3. N_2 adsorption and desorption data at 313 K.

PAF-5		PEI (10 wt%)⊂PAF-5		PEI (30 wt%)⊂PAF-5		PEI (40 wt%)⊂PAF-5	
P **(atm)**	***V*** **(cc/g)**	***P*** **(atm)**	***V*** **(cc/g)**	***P*** **(atm)**	***V*** **(cc/g)**	***P*** **(atm)**	***V*** **(cc/g)**
1.27E-02	1.14E-02	1.31E-02	2.30E-03	2.62E-01	1.31E-02	6.62E-01	4.00E-03
2.28E-02	4.04E-02	2.26E-02	3.58E-02	3.12E-01	4.07E-02	7.12E-01	4.53E-02
3.26E-02	9.02E-02	3.22E-02	7.34E-02	3.62E-01	7.47E-02	7.62E-01	7.34E-02
4.24E-02	1.74E-01	4.21E-02	1.11E-01	4.12E-01	1.02E-01	8.12E-01	1.07E-01
5.22E-02	2.53E-01	5.18E-02	1.72E-01	4.62E-01	1.44E-01	8.62E-01	1.48E-01
6.22E-02	3.05E-01	6.21E-02	1.92E-01	5.12E-01	1.83E-01	9.12E-01	1.90E-01
7.22E-02	3.30E-01	7.23E-02	1.78E-01	5.62E-01	2.23E-01	9.62E-01	2.26E-01
8.24E-02	3.44E-01	8.26E-02	1.51E-01	6.12E-01	2.65E-01	9.99E-01	2.63E-01
9.29E-02	2.97E-01	9.29E-02	1.07E-01	6.62E-01	3.10E-01	9.42E-01	2.75E-01
1.12E-01	2.63E-01	1.12E-01	9.59E-02	7.12E-01	3.36E-01	8.88E-01	2.42E-01
1.62E-01	3.05E-01	1.62E-01	1.15E-01	7.62E-01	3.84E-01	8.38E-01	2.48E-01
2.12E-01	4.86E-01	2.12E-01	2.22E-01	8.12E-01	4.43E-01	7.88E-01	2.62E-01
2.62E-01	5.55E-01	2.62E-01	2.76E-01	8.62E-01	4.95E-01	7.38E-01	2.64E-01
3.11E-01	7.23E-01	3.12E-01	3.87E-01	9.12E-01	5.28E-01	6.88E-01	2.42E-01
3.61E-01	9.21E-01	3.62E-01	4.81E-01	9.62E-01	5.85E-01	6.38E-01	2.38E-01
4.12E-01	9.12E-01	4.12E-01	4.74E-01	9.99E-01	6.24E-01	5.88E-01	2.29E-01
4.62E-01	9.80E-01	4.62E-01	5.51E-01	9.43E-01	5.91E-01	5.38E-01	2.14E-01
5.12E-01	1.26E+00	5.11E-01	6.65E-01	8.88E-01	5.77E-01	4.88E-01	1.84E-01
5.62E-01	1.29E+00	5.62E-01	7.34E-01	8.38E-01	5.73E-01	4.38E-01	1.78E-01
6.11E-01	1.43E+00	6.12E-01	7.96E-01	7.88E-01	6.16E-01	3.88E-01	1.68E-01
6.62E-01	1.51E+00	6.62E-01	8.67E-01	7.38E-01	5.87E-01	3.38E-01	1.57E-01
7.11E-01	1.71E+00	7.12E-01	9.34E-01	6.88E-01	5.59E-01	2.88E-01	1.37E-01
7.62E-01	1.79E+00	7.62E-01	9.67E-01	6.38E-01	5.29E-01	2.38E-01	1.45E-01
8.11E-01	1.92E+00	8.12E-01	1.04E+00	5.88E-01	5.14E-01	1.88E-01	1.35E-01
8.61E-01	2.27E+00	8.61E-01	1.12E+00	5.38E-01	4.88E-01	1.38E-01	1.64E-01
9.12E-01	2.24E+00	9.12E-01	1.10E+00	4.88E-01	4.54E-01	8.80E-02	1.78E-01
9.62E-01	2.31E+00	9.62E-01	1.11E+00	4.38E-01	4.29E-01	3.12E-02	1.70E-01
9.99E-01	2.56E+00	9.99E-01	1.25E+00	3.88E-01	4.06E-01	3.94E-03	1.62E-01
9.38E-01	2.30E+00	9.39E-01	1.12E+00	3.38E-01	3.86E-01		
8.87E-01	2.28E+00	8.88E-01	1.15E+00	2.88E-01	3.56E-01		
8.38E-01	2.12E+00	8.38E-01	1.13E+00	2.38E-01	3.42E-01		
7.88E-01	2.09E+00	7.88E-01	1.02E+00	1.88E-01	3.20E-01		
7.38E-01	1.96E+00	7.39E-01	9.52E-01	1.38E-01	3.12E-01		
6.88E-01	1.85E+00	6.88E-01	9.38E-01	8.80E-02	2.97E-01		
6.38E-01	1.69E+00	6.38E-01	8.98E-01	3.13E-02	2.47E-01		
5.88E-01	1.59E+00	5.88E-01	8.29E-01				
5.38E-01	1.48E+00	5.38E-01	7.34E-01				

4.88E-01	1.30E+00	4.88E-01	7.01E-01
4.39E-01	1.04E+00	4.39E-01	5.16E-01
3.88E-01	1.14E+00	3.88E-01	5.52E-01
3.38E-01	1.02E+00	3.38E-01	4.86E-01
2.88E-01	8.35E-01	2.89E-01	3.98E-01
2.39E-01	5.76E-01	2.39E-01	2.77E-01
1.89E-01	4.88E-01	1.88E-01	2.14E-01
1.38E-01	4.30E-01	1.38E-01	1.91E-01

Table S4. N_2 adsorption and desorption data at 323 K.

PAF-5		PEI (10 wt%)⊂PAF-5		PEI (30 wt%)⊂PAF-5		PEI (40 wt%)⊂PAF-5	
P **(atm)**	***V*** **(cc/g)**	***P*** **(atm)**	***V*** **(cc/g)**	***P*** **(atm)**	***V*** **(cc/g)**	***P*** **(atm)**	***V*** **(cc/g)**
1.12E-01	7.50E-03	4.29E-02	2.40E-03	5.29E-02	1.40E-02	6.12E-01	6.20E-03
1.62E-01	6.78E-02	5.30E-02	1.80E-02	6.29E-02	1.60E-02	6.62E-01	3.11E-02
2.12E-01	1.29E-01	6.30E-02	2.81E-02	7.29E-02	1.08E-02	7.12E-01	5.61E-02
2.62E-01	2.18E-01	7.30E-02	3.83E-02	8.30E-02	8.70E-03	7.62E-01	8.28E-02
3.12E-01	2.88E-01	8.30E-02	4.80E-02	9.30E-02	1.04E-02	8.12E-01	1.15E-01
3.62E-01	3.83E-01	9.29E-02	6.62E-02	1.12E-01	7.60E-03	8.62E-01	1.79E-01
4.12E-01	4.45E-01	1.12E-01	9.16E-02	1.62E-01	3.40E-03	9.12E-01	1.86E-01
4.62E-01	5.47E-01	1.62E-01	1.58E-01	2.62E-01	7.20E-03	9.62E-01	2.26E-01
5.12E-01	6.63E-01	2.12E-01	2.13E-01	3.12E-01	2.21E-02	9.99E-01	2.38E-01
5.62E-01	7.24E-01	2.62E-01	3.04E-01	3.62E-01	4.26E-02	9.42E-01	2.12E-01
6.12E-01	8.35E-01	3.12E-01	3.61E-01	4.12E-01	3.28E-02	8.88E-01	2.28E-01
6.62E-01	9.54E-01	3.62E-01	4.57E-01	4.62E-01	6.72E-02	8.38E-01	2.30E-01
7.12E-01	1.03E+00	4.12E-01	5.22E-01	5.12E-01	9.27E-02	7.88E-01	2.26E-01
7.62E-01	1.14E+00	4.62E-01	6.26E-01	5.62E-01	1.09E-01	7.38E-01	1.87E-01
8.12E-01	1.25E+00	5.12E-01	7.17E-01	6.12E-01	1.34E-01	6.88E-01	2.04E-01
8.62E-01	1.38E+00	5.62E-01	8.04E-01	6.62E-01	1.58E-01	6.38E-01	1.96E-01
9.11E-01	1.55E+00	6.12E-01	9.03E-01	7.12E-01	1.87E-01	5.88E-01	2.03E-01
9.62E-01	1.63E+00	6.62E-01	9.86E-01	7.62E-01	2.16E-01	5.38E-01	1.74E-01
9.99E-01	1.71E+00	7.12E-01	1.13E+00	8.12E-01	2.84E-01	4.88E-01	1.64E-01
9.42E-01	1.69E+00	7.62E-01	1.20E+00	8.62E-01	3.27E-01	4.38E-01	1.56E-01
8.88E-01	1.60E+00	8.12E-01	1.29E+00	9.12E-01	4.04E-01	3.88E-01	1.39E-01
8.38E-01	1.50E+00	8.62E-01	1.45E+00	9.62E-01	4.24E-01	3.38E-01	1.43E-01
7.88E-01	1.41E+00	9.12E-01	1.54E+00	9.99E-01	4.68E-01	2.88E-01	1.24E-01
7.38E-01	1.34E+00	9.62E-01	1.64E+00	9.42E-01	4.72E-01	2.38E-01	1.36E-01
6.88E-01	1.23E+00	9.99E-01	1.72E+00	8.88E-01	4.94E-01	1.88E-01	1.39E-01
6.38E-01	1.12E+00	9.42E-01	1.66E+00	8.38E-01	4.77E-01	1.38E-01	1.65E-01
5.88E-01	1.03E+00	8.88E-01	1.58E+00	7.88E-01	4.84E-01	8.80E-02	1.79E-01
5.38E-01	9.98E-01	8.38E-01	1.48E+00	7.38E-01	4.96E-01	3.12E-02	1.41E-01
4.88E-01	8.59E-01	7.88E-01	1.41E+00	6.88E-01	4.79E-01		
4.38E-01	7.57E-01	7.38E-01	1.32E+00	6.38E-01	4.69E-01		
3.88E-01	6.61E-01	6.88E-01	1.25E+00	5.88E-01	4.74E-01		
3.38E-01	5.52E-01	6.38E-01	1.14E+00	5.38E-01	4.53E-01		
2.88E-01	4.48E-01	5.88E-01	1.08E+00	4.88E-01	4.29E-01		
2.38E-01	4.02E-01	5.38E-01	9.69E-01	4.38E-01	4.26E-01		
1.88E-01	3.10E-01	4.88E-01	8.62E-01	3.88E-01	4.12E-01		
1.38E-01	2.50E-01	4.38E-01	7.75E-01	3.38E-01	3.85E-01		
8.82E-02	1.75E-01	3.88E-01	7.00E-01	2.88E-01	3.88E-01		

3.14E-02	5.79E-02	3.38E-01	6.07E-01	2.38E-01	3.92E-01
		2.88E-01	5.07E-01	1.88E-01	3.93E-01
		2.38E-01	4.37E-01	1.38E-01	4.07E-01
		1.88E-01	3.54E-01	8.80E-02	4.12E-01
		1.38E-01	3.05E-01	3.09E-02	4.31E-01
		8.81E-02	2.56E-01	3.78E-03	4.22E-01
		3.14E-02	1.39E-01		

Table S5. CO_2 adsorption and desorption data at 298 K.

PAF-5		PEI (10 wt%)⊂PAF-5		PEI (30 wt%)⊂PAF-5		PEI (40 wt%)⊂PAF-5	
P **(atm)**	***V*** **(cc/g)**	***P*** **(atm)**	***V*** **(cc/g)**	***P*** **(atm)**	***V*** **(cc/g)**	***P*** **(atm)**	***V*** **(cc/g)**
1.00E-03	1.63E-02	1.00E-03	4.25E+00	1.00E-04	8.74E+00	9.98E-05	2.41E+01
2.01E-03	4.70E-02	2.00E-03	5.31E+00	1.99E-04	1.72E+01	1.99E-04	2.87E+01
3.00E-03	7.84E-02	3.05E-03	5.93E+00	2.99E-04	1.90E+01	2.99E-04	3.11E+01
4.02E-03	1.13E-01	4.08E-03	6.40E+00	4.01E-04	2.01E+01	3.99E-04	3.26E+01
5.00E-03	1.42E-01	5.11E-03	6.76E+00	5.08E-04	2.08E+01	4.99E-04	3.39E+01
6.35E-03	1.89E-01	6.05E-03	7.03E+00	6.01E-04	2.13E+01	5.99E-04	3.47E+01
7.03E-03	2.08E-01	7.13E-03	7.30E+00	7.00E-04	2.19E+01	7.01E-04	3.55E+01
9.12E-03	2.86E-01	8.25E-03	7.56E+00	8.06E-04	2.28E+01	8.00E-04	3.62E+01
1.04E-02	6.26E-01	9.09E-03	7.73E+00	9.02E-04	2.33E+01	9.00E-04	3.68E+01
1.25E-02	6.77E-01	1.01E-02	7.91E+00	1.01E-03	2.39E+01	1.00E-03	3.72E+01
2.19E-02	1.07E+00	2.01E-02	8.95E+00	2.01E-03	2.67E+01	2.02E-03	4.00E+01
3.15E-02	1.60E+00	3.06E-02	9.82E+00	3.00E-03	2.82E+01	3.01E-03	4.19E+01
4.15E-02	2.07E+00	4.09E-02	1.06E+01	4.04E-03	2.93E+01	4.03E-03	4.31E+01
5.12E-02	2.54E+00	5.11E-02	1.12E+01	5.12E-03	3.04E+01	5.02E-03	4.42E+01
6.13E-02	2.91E+00	6.13E-02	1.18E+01	6.01E-03	3.10E+01	6.05E-03	4.51E+01
7.17E-02	3.21E+00	7.14E-02	1.25E+01	7.06E-03	3.16E+01	7.08E-03	4.58E+01
8.19E-02	3.61E+00	8.15E-02	1.30E+01	8.06E-03	3.21E+01	8.13E-03	4.64E+01
9.25E-02	3.89E+00	9.16E-02	1.36E+01	9.12E-03	3.26E+01	9.10E-03	4.69E+01
1.11E-01	4.48E+00	1.10E-01	1.44E+01	1.02E-02	3.31E+01	1.02E-02	4.74E+01
1.59E-01	6.25E+00	1.57E-01	1.65E+01	2.07E-02	3.48E+01	2.01E-02	4.88E+01
2.08E-01	8.07E+00	2.06E-01	1.86E+01	3.15E-02	3.63E+01	3.05E-02	5.03E+01
2.59E-01	9.78E+00	2.56E-01	2.08E+01	3.96E-02	3.72E+01	4.08E-02	5.16E+01
3.09E-01	1.16E+01	3.06E-01	2.30E+01	4.93E-02	3.82E+01	5.11E-02	5.29E+01
3.58E-01	1.35E+01	3.57E-01	2.51E+01	5.95E-02	3.91E+01	5.92E-02	5.37E+01
4.09E-01	1.52E+01	4.07E-01	2.69E+01	6.99E-02	3.99E+01	7.14E-02	5.49E+01
4.59E-01	1.69E+01	4.57E-01	2.86E+01	7.98E-02	4.07E+01	7.97E-02	5.56E+01
5.08E-01	1.87E+01	5.08E-01	3.03E+01	9.05E-02	4.14E+01	8.95E-02	5.64E+01
5.58E-01	2.03E+01	5.58E-01	3.19E+01	1.08E-01	4.25E+01	1.07E-01	5.75E+01
6.09E-01	2.20E+01	6.08E-01	3.35E+01	1.53E-01	4.47E+01	1.51E-01	5.98E+01
6.59E-01	2.36E+01	6.58E-01	3.50E+01	2.03E-01	4.70E+01	2.01E-01	6.20E+01
7.08E-01	2.52E+01	7.08E-01	3.65E+01	2.55E-01	4.89E+01	2.52E-01	6.41E+01
7.59E-01	2.68E+01	7.58E-01	3.80E+01	3.05E-01	5.09E+01	3.03E-01	6.62E+01
8.09E-01	2.84E+01	8.08E-01	3.94E+01	3.56E-01	5.26E+01	3.55E-01	6.78E+01
8.58E-01	3.00E+01	8.58E-01	4.08E+01	4.07E-01	5.39E+01	4.06E-01	6.92E+01
9.09E-01	3.14E+01	9.08E-01	4.23E+01	4.57E-01	5.52E+01	4.57E-01	7.03E+01
9.59E-01	3.29E+01	9.58E-01	4.36E+01	5.08E-01	5.62E+01	5.07E-01	7.13E+01
9.99E-01	3.44E+01	9.99E-01	4.49E+01	5.58E-01	5.73E+01	5.57E-01	7.23E+01

9.42E-01	3.27E+01	9.43E-01	4.35E+01	6.08E-01	5.84E+01	6.08E-01	7.32E+01
8.90E-01	3.13E+01	8.91E-01	4.24E+01	6.58E-01	5.94E+01	6.59E-01	7.40E+01
8.41E-01	3.00E+01	8.41E-01	4.12E+01	7.09E-01	6.02E+01	7.08E-01	7.48E+01
7.91E-01	2.85E+01	7.91E-01	3.99E+01	7.60E-01	6.09E+01	7.59E-01	7.55E+01
7.41E-01	2.69E+01	7.41E-01	3.87E+01	8.09E-01	6.18E+01	8.08E-01	7.63E+01
6.91E-01	2.54E+01	6.92E-01	3.74E+01	8.59E-01	6.26E+01	8.60E-01	7.68E+01
6.41E-01	2.38E+01	6.41E-01	3.60E+01	9.09E-01	6.34E+01	9.08E-01	7.76E+01
5.91E-01	2.24E+01	5.92E-01	3.46E+01	9.60E-01	6.40E+01	9.60E-01	7.82E+01
5.41E-01	2.07E+01	5.42E-01	3.32E+01	9.99E-01	6.48E+01	9.99E-01	7.87E+01
4.91E-01	1.92E+01	4.92E-01	3.17E+01	9.40E-01	6.44E+01	9.41E-01	7.85E+01
4.42E-01	1.74E+01	4.42E-01	3.02E+01	8.89E-01	6.41E+01	8.88E-01	7.83E+01
3.91E-01	1.60E+01	3.92E-01	2.85E+01	8.39E-01	6.37E+01	8.39E-01	7.81E+01
3.41E-01	1.42E+01	3.42E-01	2.68E+01	7.89E-01	6.33E+01	7.89E-01	7.79E+01
2.92E-01	1.24E+01	2.93E-01	2.49E+01	7.39E-01	6.28E+01	7.39E-01	7.76E+01
2.42E-01	1.04E+01	2.43E-01	2.28E+01	6.89E-01	6.23E+01	6.89E-01	7.73E+01
1.91E-01	8.60E+00	1.94E-01	2.07E+01	6.40E-01	6.18E+01	6.39E-01	7.69E+01
1.41E-01	6.76E+00	1.44E-01	1.85E+01	5.90E-01	6.12E+01	5.89E-01	7.65E+01
		9.41E-02	1.62E+01	5.40E-01	6.06E+01	5.39E-01	7.61E+01
		4.24E-02	1.32E+01	4.90E-01	5.99E+01	4.89E-01	7.56E+01
				4.40E-01	5.92E+01	4.40E-01	7.51E+01
				3.90E-01	5.83E+01	3.90E-01	7.45E+01
				3.41E-01	5.74E+01	3.40E-01	7.38E+01
				2.92E-01	5.61E+01	2.91E-01	7.28E+01
				2.43E-01	5.45E+01	2.42E-01	7.15E+01
				1.93E-01	5.30E+01	1.93E-01	7.03E+01
				1.43E-01	5.15E+01	1.43E-01	6.90E+01
				9.54E-02	4.95E+01	9.52E-02	6.74E+01
				4.64E-02	4.63E+01	4.75E-02	6.46E+01
				7.51E-03	3.73E+01	8.38E-03	5.59E+01
						4.53E-03	5.23E+01
						9.87E-04	4.25E+01

Table S6. CO_2 adsorption and desorption data at 313 K.

PAF-5		PEI (10 wt%)⊂PAF-5		PEI (30 wt%)⊂PAF-5		PEI (40 wt%)⊂PAF-5	
P **(atm)**	***V*** **(cc/g)**	***P*** **(atm)**	***V*** **(cc/g)**	***P*** **(atm)**	***V*** **(cc/g)**	***P*** **(atm)**	***V*** **(cc/g)**
1.03E-03	7.00E-04	1.02E-03	2.14E+00	1.03E-04	5.28E+00	1.02E-04	1.25E+01
2.02E-03	1.80E-02	2.04E-03	3.19E+00	2.02E-04	9.61E+00	2.02E-04	1.91E+01
3.05E-03	3.67E-02	3.01E-03	3.78E+00	3.03E-04	1.20E+01	3.02E-04	2.37E+01
4.01E-03	5.52E-02	4.10E-03	4.31E+00	4.06E-04	1.39E+01	4.01E-04	2.62E+01
5.03E-03	7.53E-02	5.18E-03	4.69E+00	5.04E-04	1.50E+01	5.12E-04	2.75E+01
6.03E-03	9.41E-02	6.08E-03	4.97E+00	6.09E-04	1.60E+01	6.08E-04	2.87E+01
7.27E-03	1.19E-01	7.23E-03	5.26E+00	7.12E-04	1.66E+01	7.13E-04	2.98E+01
9.30E-03	1.65E-01	8.30E-03	5.53E+00	8.05E-04	1.75E+01	8.05E-04	3.11E+01
9.84E-03	1.74E-01	9.12E-03	5.71E+00	9.03E-04	1.81E+01	9.06E-04	3.20E+01
1.25E-02	2.63E-01	1.01E-02	5.90E+00	1.01E-03	1.87E+01	1.01E-03	3.26E+01
2.24E-02	5.10E-01	1.99E-02	7.02E+00	2.01E-03	2.21E+01	2.04E-03	3.67E+01
3.25E-02	7.54E-01	3.06E-02	7.91E+00	3.03E-03	2.39E+01	3.04E-03	3.87E+01
4.20E-02	1.01E+00	4.11E-02	8.62E+00	4.06E-03	2.51E+01	4.08E-03	3.98E+01
5.21E-02	1.24E+00	5.13E-02	9.24E+00	5.07E-03	2.60E+01	5.00E-03	4.11E+01
6.24E-02	1.40E+00	6.15E-02	9.81E+00	6.19E-03	2.69E+01	6.07E-03	4.20E+01
7.22E-02	1.63E+00	7.16E-02	1.03E+01	7.24E-03	2.75E+01	7.12E-03	4.27E+01
8.21E-02	1.85E+00	8.17E-02	1.08E+01	8.08E-03	2.80E+01	8.01E-03	4.31E+01
9.26E-02	2.09E+00	9.18E-02	1.12E+01	9.03E-03	2.85E+01	9.13E-03	4.38E+01
1.11E-01	2.59E+00	1.10E-01	1.20E+01	1.01E-02	2.90E+01	1.03E-02	4.43E+01
1.59E-01	3.91E+00	1.57E-01	1.37E+01	2.06E-02	3.10E+01	1.98E-02	4.61E+01
2.11E-01	4.70E+00	2.07E-01	1.54E+01	3.12E-02	3.27E+01	2.95E-02	4.77E+01
2.60E-01	5.98E+00	2.57E-01	1.71E+01	3.95E-02	3.37E+01	3.91E-02	4.87E+01
3.10E-01	7.26E+00	3.07E-01	1.90E+01	4.94E-02	3.47E+01	5.01E-02	5.03E+01
3.60E-01	8.50E+00	3.58E-01	2.07E+01	5.95E-02	3.57E+01	6.15E-02	5.15E+01
4.10E-01	9.66E+00	4.08E-01	2.21E+01	6.99E-02	3.65E+01	7.05E-02	5.21E+01
4.60E-01	1.08E+01	4.59E-01	2.35E+01	8.10E-02	3.71E+01	7.93E-02	5.29E+01
5.10E-01	1.20E+01	5.09E-01	2.48E+01	9.07E-02	3.78E+01	8.95E-02	5.37E+01
5.59E-01	1.32E+01	5.59E-01	2.61E+01	1.08E-01	3.89E+01	1.07E-01	5.47E+01
6.09E-01	1.44E+01	6.09E-01	2.73E+01	1.54E-01	4.10E+01	1.55E-01	5.64E+01
6.60E-01	1.56E+01	6.59E-01	2.85E+01	2.05E-01	4.29E+01	2.01E-01	5.87E+01
7.09E-01	1.66E+01	7.09E-01	2.97E+01	2.55E-01	4.48E+01	2.53E-01	6.07E+01
7.60E-01	1.77E+01	7.59E-01	3.08E+01	3.05E-01	4.70E+01	3.04E-01	6.27E+01
8.09E-01	1.89E+01	8.09E-01	3.19E+01	3.57E-01	4.84E+01	3.57E-01	6.40E+01
8.59E-01	2.00E+01	8.60E-01	3.30E+01	4.08E-01	4.95E+01	4.06E-01	6.54E+01
9.09E-01	2.10E+01	9.09E-01	3.42E+01	4.57E-01	5.07E+01	4.56E-01	6.66E+01
9.60E-01	2.20E+01	9.60E-01	3.52E+01	5.09E-01	5.17E+01	5.09E-01	6.74E+01
9.99E-01	2.31E+01	9.99E-01	3.62E+01	5.58E-01	5.27E+01	5.57E-01	6.84E+01

9.40E-01	2.18E+01	9.43E-01	3.52E+01	6.09E-01	5.36E+01	6.08E-01	6.93E+01
8.89E-01	2.09E+01	8.91E-01	3.42E+01	6.60E-01	5.43E+01	6.59E-01	7.00E+01
8.40E-01	2.02E+01	8.41E-01	3.33E+01	7.09E-01	5.50E+01	7.08E-01	7.09E+01
7.90E-01	1.90E+01	7.91E-01	3.24E+01	7.58E-01	5.61E+01	7.59E-01	7.15E+01
7.40E-01	1.79E+01	7.41E-01	3.15E+01	8.10E-01	5.68E+01	8.09E-01	7.22E+01
6.90E-01	1.68E+01	6.91E-01	3.05E+01	8.61E-01	5.72E+01	8.60E-01	7.27E+01
6.39E-01	1.58E+01	6.41E-01	2.94E+01	9.10E-01	5.79E+01	9.10E-01	7.31E+01
5.90E-01	1.47E+01	5.91E-01	2.83E+01	9.59E-01	5.87E+01	9.58E-01	7.39E+01
5.40E-01	1.37E+01	5.41E-01	2.72E+01	9.99E-01	5.93E+01	9.99E-01	7.44E+01
4.90E-01	1.26E+01	4.91E-01	2.61E+01	9.40E-01	5.90E+01	9.41E-01	7.42E+01
4.41E-01	1.14E+01	4.41E-01	2.49E+01	8.89E-01	5.86E+01	8.88E-01	7.41E+01
3.90E-01	1.05E+01	3.91E-01	2.36E+01	8.39E-01	5.83E+01	8.39E-01	7.39E+01
3.40E-01	9.30E+00	3.42E-01	2.22E+01	7.89E-01	5.80E+01	7.89E-01	7.36E+01
2.90E-01	8.06E+00	2.92E-01	2.06E+01	7.40E-01	5.75E+01	7.39E-01	7.34E+01
2.41E-01	6.76E+00	2.43E-01	1.88E+01	6.89E-01	5.70E+01	6.89E-01	7.30E+01
1.89E-01	5.92E+00	1.93E-01	1.71E+01	6.39E-01	5.65E+01	6.39E-01	7.27E+01
1.39E-01	4.65E+00	1.43E-01	1.53E+01	5.89E-01	5.60E+01	5.89E-01	7.23E+01
		9.35E-02	1.34E+01	5.40E-01	5.55E+01	5.39E-01	7.19E+01
		4.18E-02	1.06E+01	4.90E-01	5.49E+01	4.91E-01	7.12E+01
				4.40E-01	5.42E+01	4.40E-01	7.07E+01
				3.90E-01	5.34E+01	3.90E-01	7.01E+01
				3.42E-01	5.23E+01	3.41E-01	6.94E+01
				2.91E-01	5.12E+01	2.92E-01	6.84E+01
				2.42E-01	4.97E+01	2.44E-01	6.69E+01
				1.93E-01	4.81E+01	1.94E-01	6.55E+01
				1.44E-01	4.64E+01	1.44E-01	6.42E+01
				9.70E-02	4.41E+01	9.81E-02	6.21E+01
				4.86E-02	4.05E+01	5.10E-02	5.87E+01
				8.03E-03	3.09E+01	7.88E-03	4.79E+01
						4.46E-03	4.42E+01
						9.77E-04	3.40E+01

Table S7. CO_2 adsorption and desorption data at 323 K.

PAF-5		PEI (10 wt%)⊂PAF-5		PEI (30 wt%)⊂PAF-5		PEI (40 wt%)⊂PAF-5	
P **(atm)**	***V*** **(cc/g)**	***P*** **(atm)**	***V*** **(cc/g)**	***P*** **(atm)**	***V*** **(cc/g)**	***P*** **(atm)**	***V*** **(cc/g)**
1.10E-03	5.90E-03	1.03E-03	8.61E-01	1.04E-04	9.48E-01	1.04E-04	2.31E+00
2.11E-03	3.00E-02	2.08E-03	1.59E+00	2.07E-04	2.67E+00	2.02E-04	6.32E+00
3.19E-03	5.33E-02	3.04E-03	2.06E+00	3.04E-04	4.60E+00	3.02E-04	1.07E+01
4.26E-03	7.64E-02	4.19E-03	2.49E+00	4.08E-04	6.07E+00	4.07E-04	1.38E+01
5.33E-03	1.01E-01	5.15E-03	2.80E+00	5.02E-04	7.43E+00	5.13E-04	1.67E+01
6.41E-03	1.23E-01	6.25E-03	3.10E+00	6.05E-04	8.87E+00	6.10E-04	1.87E+01
7.49E-03	1.47E-01	7.25E-03	3.40E+00	7.03E-04	9.99E+00	7.05E-04	2.06E+01
8.55E-03	1.70E-01	8.12E-03	3.59E+00	8.07E-04	1.10E+01	8.08E-04	2.23E+01
9.62E-03	1.95E-01	9.17E-03	3.80E+00	9.08E-04	1.18E+01	9.08E-04	2.38E+01
1.07E-02	2.19E-01	1.02E-02	4.01E+00	1.05E-03	1.27E+01	1.00E-03	2.50E+01
2.26E-02	5.07E-01	2.06E-02	5.19E+00	2.06E-03	1.74E+01	2.10E-03	3.15E+01
3.24E-02	7.34E-01	3.11E-02	6.05E+00	3.01E-03	1.99E+01	3.06E-03	3.48E+01
4.26E-02	9.81E-01	4.14E-02	6.78E+00	4.14E-03	2.16E+01	4.06E-03	3.69E+01
5.25E-02	1.23E+00	5.16E-02	7.42E+00	5.06E-03	2.26E+01	5.03E-03	3.76E+01
6.26E-02	1.48E+00	6.18E-02	7.97E+00	6.06E-03	2.36E+01	6.22E-03	3.92E+01
7.26E-02	1.72E+00	7.20E-02	8.46E+00	7.16E-03	2.43E+01	7.11E-03	4.01E+01
8.26E-02	1.98E+00	8.19E-02	8.96E+00	8.04E-03	2.51E+01	8.06E-03	4.10E+01
9.26E-02	2.22E+00	9.21E-02	9.40E+00	9.28E-03	2.57E+01	9.29E-03	4.16E+01
1.11E-01	2.66E+00	1.11E-01	1.01E+01	1.02E-02	2.62E+01	1.03E-02	4.23E+01
1.60E-01	3.79E+00	1.59E-01	1.17E+01	2.02E-02	2.87E+01	1.91E-02	4.47E+01
2.09E-01	5.00E+00	2.08E-01	1.34E+01	3.06E-02	3.05E+01	2.99E-02	4.65E+01
2.58E-01	6.58E+00	2.58E-01	1.54E+01	3.94E-02	3.16E+01	4.03E-02	4.80E+01
3.08E-01	8.32E+00	3.08E-01	1.75E+01	4.91E-02	3.27E+01	5.14E-02	4.93E+01
3.59E-01	9.62E+00	3.59E-01	1.91E+01	6.02E-02	3.35E+01	6.05E-02	5.00E+01
4.10E-01	1.08E+01	4.09E-01	2.04E+01	6.94E-02	3.45E+01	6.91E-02	5.09E+01
4.60E-01	1.19E+01	4.59E-01	2.17E+01	8.11E-02	3.51E+01	7.99E-02	5.16E+01
5.10E-01	1.29E+01	5.10E-01	2.29E+01	9.12E-02	3.56E+01	8.95E-02	5.24E+01
5.60E-01	1.39E+01	5.60E-01	2.40E+01	1.07E-01	3.69E+01	1.08E-01	5.33E+01
6.10E-01	1.49E+01	6.10E-01	2.52E+01	1.57E-01	3.85E+01	1.53E-01	5.52E+01
6.60E-01	1.59E+01	6.60E-01	2.63E+01	2.04E-01	4.06E+01	2.03E-01	5.71E+01
7.10E-01	1.69E+01	7.10E-01	2.74E+01	2.55E-01	4.25E+01	2.55E-01	5.87E+01
7.60E-01	1.78E+01	7.60E-01	2.84E+01	3.07E-01	4.42E+01	3.05E-01	6.05E+01
8.10E-01	1.88E+01	8.09E-01	2.95E+01	3.56E-01	4.59E+01	3.56E-01	6.20E+01
8.60E-01	1.98E+01	8.60E-01	3.04E+01	4.08E-01	4.70E+01	4.09E-01	6.28E+01
9.10E-01	2.06E+01	9.10E-01	3.14E+01	4.59E-01	4.78E+01	4.55E-01	6.41E+01
9.60E-01	2.16E+01	9.59E-01	3.25E+01	5.07E-01	4.90E+01	5.09E-01	6.49E+01

9.99E-01	2.23E+01	9.99E-01	3.33E+01	5.61E-01	4.96E+01	5.58E-01	6.57E+01
9.43E-01	2.14E+01	9.42E-01	3.24E+01	6.06E-01	5.09E+01	6.10E-01	6.63E+01
8.90E-01	2.06E+01	8.89E-01	3.16E+01	6.60E-01	5.15E+01	6.58E-01	6.70E+01
8.40E-01	1.98E+01	8.40E-01	3.08E+01	7.10E-01	5.21E+01	7.09E-01	6.76E+01
7.90E-01	1.90E+01	7.90E-01	2.97E+01	7.59E-01	5.29E+01	7.60E-01	6.81E+01
7.40E-01	1.81E+01	7.39E-01	2.89E+01	8.10E-01	5.35E+01	8.09E-01	6.87E+01
6.90E-01	1.73E+01	6.89E-01	2.81E+01	8.60E-01	5.41E+01	8.61E-01	6.91E+01
6.40E-01	1.64E+01	6.40E-01	2.72E+01	9.09E-01	5.50E+01	9.09E-01	6.97E+01
5.90E-01	1.54E+01	5.90E-01	2.62E+01	9.61E-01	5.53E+01	9.60E-01	7.02E+01
5.40E-01	1.45E+01	5.40E-01	2.52E+01	9.99E-01	5.61E+01	9.99E-01	7.06E+01
4.90E-01	1.35E+01	4.90E-01	2.41E+01	9.39E-01	5.58E+01	9.40E-01	7.06E+01
4.40E-01	1.25E+01	4.40E-01	2.30E+01	8.89E-01	5.55E+01	8.88E-01	7.05E+01
3.90E-01	1.14E+01	3.90E-01	2.18E+01	8.39E-01	5.50E+01	8.39E-01	7.02E+01
3.40E-01	1.03E+01	3.40E-01	2.05E+01	7.89E-01	5.47E+01	7.89E-01	7.00E+01
2.91E-01	8.98E+00	2.91E-01	1.90E+01	7.39E-01	5.44E+01	7.38E-01	6.99E+01
2.42E-01	7.24E+00	2.42E-01	1.69E+01	6.89E-01	5.40E+01	6.89E-01	6.97E+01
1.91E-01	5.70E+00	1.92E-01	1.50E+01	6.40E-01	5.33E+01	6.39E-01	6.94E+01
1.41E-01	4.47E+00	1.41E-01	1.33E+01	5.89E-01	5.28E+01	5.89E-01	6.91E+01
9.07E-02	3.26E+00	9.21E-02	1.14E+01	5.39E-01	5.23E+01	5.40E-01	6.86E+01
3.52E-02	1.79E+00	3.93E-02	8.54E+00	4.90E-01	5.18E+01	4.90E-01	6.82E+01
5.72E-03	8.41E-01	9.74E-03	4.96E+00	4.40E-01	5.11E+01	4.40E-01	6.77E+01
				3.91E-01	5.02E+01	3.91E-01	6.70E+01
				3.42E-01	4.91E+01	3.40E-01	6.63E+01
				2.92E-01	4.79E+01	2.92E-01	6.53E+01
				2.43E-01	4.64E+01	2.44E-01	6.38E+01
				1.94E-01	4.47E+01	1.93E-01	6.26E+01
				1.44E-01	4.31E+01	1.45E-01	6.10E+01
				9.80E-02	4.06E+01	9.87E-02	5.88E+01
				4.93E-02	3.68E+01	5.12E-02	5.53E+01
				8.42E-03	2.69E+01	7.93E-03	4.32E+01

국문 초록

동공을 변형시킨 다공성 유기 고분자를 이용한 이산화탄소 흡착 연구

최근 나타나는 지구 온난화, 기후 변화, 그리고 해양의 산성화와 같은 환경적인 위기를 경감시키기 위해서 매연으로부터 이산화탄소를 효과적으로 포집하는 기술의 개발이 매우 중요하다.[1-4] 공장에서부터 배출되는 산업 매연은 주로 질소 (75%)와 이산화탄소 (15%) 그리고 수증기를 포함하는 여러가지 기체들로 구성되어 있으며, 313 K 와 323 K 사이의 온도에서 배출된다.[1] 따라서, 낮은 이산화탄소 분압에서 질소에 대한 이산화탄소의 높은 선택성과 물에 대한 뛰어난 안정성, 그리고 높은 온도에서 높은 이산화탄소 흡착량을 가지는 물질을 개발하는 것이 매우 중요하다.[1] 다공성 유기 고분자는 높은 표면적, 매우 낮은 밀도 그리고 뛰어난 열적 화학적 안정성과 같은 뛰어난 물리적 성질로 인하여 새로운 이산화탄소 포집 물질로 많은 각광을 받았다.[5-9] 특히, C, N, H와 같은 가벼운 원소들의 공유결합으로 얻어지는 다공성 유기 고분자의 낮은 밀도는 포집체 단위 g당 높은 이산화탄소 포집량을 나타내게 한다.[8,9] 더욱이 다공성 유기 고분자는 물에 대해 매우 뛰어난 안정성을 나타내는데 이와 같은 특성은 연소 후 이산화탄소 포집 방법에 활용되는 물질에 필요한 성질이다. 따라서 다공성 유기 고분자는 질소에 대한 이산화탄소의 높은 선택성만 지닌다면 매우 훌륭한 이산화탄소 포집 물질이 될 수 있다. 이번 연구에서, 이산화탄소 흡착량과 질소에 대한 이산화탄소 선택성을 증가시키기 위해서 낮은 밀도와 물에 대한 우수한 안정성을 지닌 다공성 유기 고분자인 PAF-5에 폴리에틸린이민 (PEI, Mw = 800)을 주입하였다. 페닐 고리로만 이루어진 유각형 구조의 평면들이 쌓여 만들어진 이차원 구조의 PAF-5는 높은 표면

적 (BET: 1503 $m^2 g^{-1}$)과 큰 동공 너비 (1.66nm) 그리고 큰 동공 부피 (1.35 cc g-1)[11] 를 가진다. 우리는 PAF-5의 큰 1D 채널에 퍼져있는 PEI의 많은 아민 그룹이 강한 이산화탄소의 상호작용 장소로 역할을 할 것이라고 생각하였다. 특히 PEI(40 wt%)⊂PAF-5는 15% 부피의 이산화 탄소가 섞여 있는 이산화탄소/질소 혼합가스로부터 313 K에서 10.0 wt%의 이산화탄소를 20분만에 흡착하였다. 이 흡착제는 질소 분위기하에 343 K에서 완전히 재생되었으며 10 주기의 흡착과 탈착 실험 이후에도 흡착제의 무게감소나 이산화탄소 흡착량의 감소를 나타내지 않았다. 313 K에서 수증기에 7일간 노출시킨 뒤에도 PEI(40 wt%)⊂PAF-5는 똑같은 양의 이산화탄소를 흡착하여 물에 대한 강한 안정성을 타나내었다.

주 요 어: 다공성 유기 고분자 • 폴리에틸린아민 • 이산화탄소 포집 •gas cycling experiment • 이산화탄소 흡착열